The Vanilloid Receptor: localization, function, and its potential as a new target for the treatment of pain

PhD Thesis

László J. Kárai, M.D.

Department of Neurology
Faculty of Medicine, University of Szeged
Hungary

2006

I dedicate this work to my family, especially to my grandmother, Ilona Sinko and to her husband, my late grandfather Laszlo M. Karai, for their devotion, love and care throughout my life.

THE THESIS IS BASED ON THE FOLLOWING PAPERS

1. Karai L, Brown DC, Mannes AJ, Connelly ST, Brown J, Gandal M, Wellisch OM, Neubert JK, Olah Z, Iadarola MJ. Deletion of vanilloid receptor-1 expressing primary afferent neurons for pain control.
J Clin Invest. 2004 May;113(9):1344-52.

2. Karai LJ, Russell JT, Iadarola MJ, Olah Z.
Vanilloid receptor 1 regulates multiple calcium compartments and contributes to Ca^{2+}-induced Ca^{2+} release in sensory neurons.
J Biol. Chem., 2004; 16;279, 16377-87.

3. R.M. Caudle, L. Karai, N. Mena, B.Y. Cooper, A.J. Mannes, F.M. Perez, M.J. Iadarola, Z. Olah
Resiniferatoxin Induced Loss of Plasma Membrane in Vanilloid Receptor Containing Cells
Neurotoxicology. 2003 Dec; 24(6):895-908.

4. Neubert JK, Karai L, Jun JH, Kim HS, Olah Z, Iadarola MJ (2003)
Peripherally Induced Resiniferatoxin Analgesia.
Pain. 2003; 104(1-2): 219-228.

5. Olah Z, Szabo T, Karai L, Hough C, Fields RD, Caudle RM, Blumberg PM, Iadarola MJ.
Ligand-induced dynamic membrane changes and cell deletion conferred by vanilloid receptor 1.
J. Biol. Chem., 2001; 14;276, 11021-11030

SUMMARY

The vanilloid receptor (TRPV1 or VR1) belongs to the transient receptor potential (TRP) channel superfamily of ion channels. It is expressed almost exclusively in a subset of sensory neurons in the dorsal root and trigeminal ganglia (DRG, TG), which give rise of C and A∂-type of primary afferent nociceptive fibers. These fibers create a dense three-dimensional meshwork in our body, which instantaneously notifies us about harmful stimuli, but can also cripple those of us who suffer from painful neurologic conditions, inflammation or malignant disease associated pain. Severe pain is still managed by opioids, sodium channel blockers or non-selective neuroablative treatments. Although, they can provide relief, their serious side effects, or *non-selective* complications, such as impaired consciousness, and compromised motor, bladder or bowel function can limit their effective use and erode quality of life. TRPV1 is one of the most important transducer and integrator of nociceptive signaling and understanding its molecular science can provide better pain-treatment options that preserve epicritic and kinesthetic sensations, motor control and consciousness.

The initial molecular biological studies in the thesis compared the wild type receptor with various modified TRPV1 molecules including the one tagged with the enhanced green fluorescent protein (eGFP). Live-cell confocal imaging on the TRPV1-eGFP fusion molecule showed the same molecular biological and electrophysiological characteristics as the wild type receptor. Direct visualization of TRPV1-eGFP disclosed sub-cellular localization of the receptor to the plasma membrane including the microvilli, and to the endoplasmic reticulum (ER). This later representation was confirmed by the overlap of TRPV1-eGFP with the vital ER-Tracker dye and indirectly by calcium imaging techniques in DRG cultures. Although, the ER localization of TRPV1 may not be surprising, due to protein synthesis in general, finding functionally active receptor at this site by using fluorescent calcium imaging was a new finding.

In the TRPV1 transfected cells (transiently or permanently) activation with potent vanilloid agonists capsaicin (CAP) and resiniferatoxin (RTX) resulted in an abrupt change in the structure of the plasma and ER membranes together with a change in shape of the mitochondria, which "rounded up" into spherical particles in contrast to their normal filiform contour. The fragmentation of intracellular organelles was shown to be due to calcium cytotoxicity and ultimately led to the demise of the TRPV1 expressing cells (heterologously TRPV1 expressing cells, and a subset of DRG neurons). By exploiting the specific expression of TRPV1 in nociceptive neurons and their selective susceptibility to vanilloid agonists especially the ultrapotent RTX, it was possible to literally kill a subset of pain-sensing

primary neurons. The treatment was selective, only the vanilloid-sensitive neurons were eliminated, other somatosensory neurons remained intact.

Based on the cellular and in vitro findings we developed a new model system in rats and dogs applicable to intractable pain in humans. It was found that peripheral (close to nerve endings) application of RTX led to degeneration of the peripheral nerve endings, followed by regeneration with no apparent change or damage of neuronal perikarya innervating the specific area. Accordingly, the effect was transient elimination of pain lasting only for several weeks. Intraganglionic or intrathecal application of RTX, however, led to selective degeneration and elimination of TRPV1 expressing neurons as confirmed by histological and immunohistochemical techniques. Animals treated this way exhibited permanent diminution or loss of pain sensation. To bridge the nonclinical rodent data and the eventual human trials we introduced a clinical canine model. Results on the veterinary canine patient population underscore the effectivenes of the treatment in real clinical conditions and reinforce the idea that it will be safe and effective. Furthermore, experimental data obtained from human dorsal root ganglion neuron cultures provide additional translational observations and argue for the applicability of the treatment in human conditions.

The intervention according to the clinical scenario can be reversible or irreversible and be applied in an anatomically targeted way. If RTX is injected to the periphery it leads to *transient* nerve terminal inactivation, which is followed by regeneration of the fibers and return of the sensation in approximately three weeks. *Irreversible* effect (permanent analgesia) can be obtained by intraganglionic or intrathecal administration of RTX (close to the neuronal cell body), which results in selective neuronal death. Both peripheral and central application of RTX achieved remarkabe reduction in pain sensation. The former can help people with conditions like painful neuromas, neuropathic and post-irradiation pain, whereas the later can stop the suffering of patients with malignant metastatic disease-associated pain. The treatment can be anatomically targeted to the desired site and according to the animal and human experimental data, it is expected that other sensory modalities and locomotion would remain intact.

Taken together, the thesis presents data on a new translational approach for the treatment of pain. It originates from basic molecular, cell biological, electrophysiological and imaging observations and uses experimental rodent and clinical canine data, together with calcium imaging studies on human dorsal root ganglion neurons to demonstrate possible human applications and the efficacy, specificity, and safety of RTX. All of these observations indicate that the RTX neuronal deletion method is a promising new interventional strategy for treating severe pain.

ACRONYMS AND ABBREVIATIONS

$[Ca^{2+}]_i$	concentration of free intracellular calcium level
$[Ca^{2+}]_o$	concentration of extracellular calcium
CAP	capsaicin
CPZ	capsazepine
CSF	cerebrospinal fluid
DRG	dorsal root ganglion
ECM	extracellular matrix
eGFP	enhanced green fluorescent protein
ER	endoplasmic reticulum
Fluo-4 AM	fluorescent Ca^{2+} indicator
HBSS	Hanks' Balanced Salt Solution
HBSSH	Hanks' Balanced Salt Solution buffered with HEPES
hTRPV1	human vanilloid 1 receptor
IM	Imaging Medium (IM): HEPES buffered (pH 7.4) Hanks' Balanced Salt Solution, supplemented with 0.01 % bovine serum albumin, 1.25 mM $CaCl_2$, 0.8 mM $MgCl_2$, 1 mM ascorbic acid, 1 mM pyruvate
INDO AM	fluorescent Ca^{2+} indicator
IR	immunoreactive
IT	intrathecal
PM	plasma membrane
RTX	resiniferatoxin
TRPV1	vanilloid receptor 1
TRPV1-eGFP	C-terminally GFP epitope-tagged TRPV1 protein
TRPV1 ε-MTH	Protein kinase C epsilon epitope tagged TRPV1
TRPV1ε-NIH3T3	cells permanently expressing the C-terminally ε-epitope tagged TRPV1
$TRPV1_{ER}$	endoplasmic reticulum localized TRPV1
$TRPV1_{PM}$	plasma membrane localized TRPV1
VAS	visual analogue scale
VR1	vanilloid receptor 1 (TRPV1)

TABLE OF CONTENTS

1. INTRODUCTION

In patient populations ranging from pediatric to the elderly, control of severe pain with currently available analgesics is frequently less than optimal [1-3]. Opioids remain the mainstay of treatment for moderate to severe pain, but they cannot universally provide relief. Some patients with cancer have pain that is refractory to conventional medical therapies including opioid analgesia, and many of them experience aversive, dose-limiting side effects. Despite more than 100 years of searching for new pharmacological modalities to treat severe pain[4-6], only very few have emerged, and the current alternatives to opioids are nonselective chemical or surgical neuroablative interventions and palliative sedation [7-9]. Both options are unsatisfactory, however. With neuroablative interventions, neurons responsible for motor, bladder, and bowel function may be indiscriminately destroyed, while with palliative sedation there is loss of consciousness; in both cases, quality of life is potentially compromised [10-13].

The specific gene expression patterns in nociceptive, mainly small unmyelinated C-fiber neurons localized in sensory ganglia offered a different approach. These neurons transduce sensations generated by noxious heat and endogenous inflammatory algesic substances and express high levels of the recently cloned transient receptor potential cation channel, subfamily V, member 1 (TRPV1; also known as the vanilloid receptor, VR1) a sodium/calcium ion channel, as compared with other sensory neurons in the DRG and trigeminal ganglia (TG) [14-16]. Molecular biological and imaging studies provided means to investigate more fully the molecular and cell biological mechanisms of pain signal transduction and the processes underlying susceptibility of TRPV1-expressing cells to impairment upon exposure to vanilloid agonists [15, 16]. Direct live-cell imaging of ectopically TRPV1-expressing cells and primary DRG cultures demonstrated that resiniferatoxin (RTX), a potent TRPV1 agonist [17], causes a large, prolonged increase in the free intracellular calcium concentration ($[Ca^{2+}]_i$). The resulting calcium cytotoxicity rapidly compromised and then deleted only the TRPV1-expressing cells or neurons [18]. These data provided a mechanistic rationale for therapeutic intervention in which application of RTX in the vicinity of DRG or TG neuronal cell bodies in vivo would selectively delete TRPV1+ neurons, thereby eliminating sensitivity to nociceptive input associated mainly with inflammation, hyperalgesia, and cancer-related pain. Other sensory modalities mediated by neurons not expressing TRPV1 would remain unaffected (e.g., proprioception and high-threshold mechanosensation). The in vitro results with RTX promised high efficacy upon in vivo administration of the drug. Experiments were designed to test peripheral and central

actions of RTX and to mimic as close as possible the various clinical scenarios in patients suffering from severe intractable pain. The central application was divided into two groups as single ganglionic and multiganglionic treatments. The former would test the efficacy and anatomical targeting of the procedure in conditions affecting a single or only a few ganglia, such as trigeminal neuralgia, herpes zoster, or Pancoast tumor. The later is designed to simulate treatment conditions possible in patients with advanced metastatic malignant disease. The procedures were tested on multiple animal species and invaluable data were collected from canine patients suffering from naturally occurring painful conditions such as malignant disease or arthritis. Upon central application of the drug (intraganglionic, intrathecal injections) the effect expected to be permanent, since RTX was administered to the vicinity of the neuronal cell body. The effect of the peripheral injections, however were anticipated to be only transient and be followed by full recovery of sensory modalities. The peripheral studies were performed in rats and as expected resulted in robust, but reversible analgesic effect in a range of painful experimental conditions. Peripheral injection would be used in conditions such as peripheral neuromas (Morton's neuroma), diabetic neuropathy, or simply after closing surgical wounds. This latter could help to reduce postoperative pain associated with major surgeries. This would also lead to reduced use of analgesics and quicker, symptom free recovery [19].

The thesis is based on rational evolution of experiments spanning between basic molecular and in vitro imaging data to relevant in vivo findings from canine patients with naturally occurring painful clinical conditions. High-resolution confocal microscopy and calcium imaging experiments endow with new information on the cellular localization of the vanilloid receptor and provide "real-time" data on the subcellular changes associated with TRPV1 activation. Additionally, findings presented below argue for the efficacy, highly specific anatomical targetability of RTX treatment, as well as provide information on the safety of the drug. There is an undeniable need for additional work to understand more the actions of vanilloids in painful conditions, however the presented data may serve as a useful starting point for future studies.

2. MATERIALS AND METHODS

2.1. Molecular Studies and Imaging Methods

2.1.1. RT-PCR Cloning and Epitope Tagging

To obtain TRPV1-specific mRNA, 100 DRGs were rapidly removed from 12 adult Harlan Sprague-Dawley rats. Total RNA was isolated with the TRI REAGENT (Molecular

Research Center Inc., Cincinnati, OH). A fragment, comprising the sequence between the XbaI and AflIII sites of rat TRPV1, was amplified first by the Access RT-PCR system (Promega) and then cloned into the BlueScript vector (Stratagene). The missing 5'-sequence was added likewise with the SacI and XbaI sites. At the 5' ends of the N- and C-terminal fragments, the SacI and AflIII sites were incorporated with forward primers AGATCTCGAGCTCAAATGGAACAACGGGCTAGCTTAGACTC and CTGTATTCCACATGTCTGGAGCTGTTCAAGTTC, respectively. As reverse primers ACTGAGTCCCGGGCGCTGATGTCTGCAGGCT and ACACAGTCGACTTTCTCCCCTGGGACCATGGAATCCTT were used, in which the XbaI and SalI sites were incorporated, respectively. The SacI-AflIII sites and the RT-PCR generated AflIII-SalI fragments were triple-ligated into a SacI and SalI cut pEGFP-N3 vector (CLONTECH). The immediate early promoter of the cytomegalovirus in the pEGFP-N3 vector was employed to produce the full-length TRPV1 with the eGFP tag. Rat TRPV1 with the short, 12-amino acid ε-tag (KGFSYFGEDLMP) was constructed in a vector, pεMTH, driven by the metallothionein promoter [20]. Briefly, SalI and MluI restriction endonuclease sites were incorporated into the TRPV1 PCR fragment amplified using the forward AGTAGTGTCGACGAACAACGGGCTAGCTTAGACTCA and reverse TTGTTGACGCGTTTTCTCCCCTGGGACCATGGAATC primers, respectively. After cutting the PCR fragment with these enzymes the size-separated cDNA insert was ligated in pεMTH at the compatible XhoI and MluI sites [20]. The chimeric constructs were verified by sequencing and transiently transfected in COS7, HEK293, and NIH 3T3 cells employing the protocol provided for the LipofectAMINE reagent (Life Technologies, Inc.). The basal activity of the pεMTH promoter was used in NIH 3T3 cells to produce TRPV1-εMTH, yet prevent toxicity from long term, high level expression of TRPV1.

2.1.2. Electrophysiology

For patch clamp studies, TRPV1eGFP-expressing COS7 and HEK293 cells were voltage-clamped in Krebs buffer containing (in mM) NaCl (124), KCl (4.9), KH_2PO_4 (1.2), $MgSO_4$ (2.4), $CaCl_2$ (2.5), $NaHCO_3$ (25.6), and glucose (10), using an Axopatch 200B amplifier (Axon Instruments, Foster City, CA). Recordings were carried out with patch electrodes (2–10 MV) filled with 10 mM HEPES buffer (pH7.4) containing (in mM) CsCl (120), tetraethylammonium chloride (20), $CaCl_2$ (1), $MgCl_2$ (2), EGTA (10), ATP (4), and GTP (0.5).

2.1.3. Western Blotting

Total protein extracts were prepared in denaturing SDS buffer and analyzed for immunoreactivity by Western blotting. TRPV1-specific antibody was raised in rabbits employing the N-terminal MEQRASLDSEESESPPQE peptide of rat TRPV1 conjugated to keyhole limpet hemocyanin as immunogen. Immune sera were affinity purified against the peptide used for immobilization. The specific antibody fraction eluted from the affinity column was diluted 1000-fold for further characterization in Western blot and immunocytochemistry experiments. This antibody fraction recognizes the native rat TRPV1. Stripping of nitrocellulose blotting filters (Bio-Rad) was carried out in 200 ml of 50 mM Tris-HCl buffer (pH 7.5) containing 2% SDS and 0.1 β-mercaptoethanol at 65 °C for 1 h. Stripped blots were reanalyzed for tagged fusion proteins either with the GFP (CLONTECH) or the εPKC-specific antibodies (Life Technologies, Inc.), prepared in rabbits. To assess equal loading, filters were re-probed with a rat cytochrome *c*-specific monoclonal antibody (6H2.B4) as suggested by the manufacturer (Transduction Laboratories). Antibodies for Western blotting were used at a 1:1000 dilution. To visualize the interaction with the primary antibodies, enhanced chemiluminescence technology was employed according to the protocol provided by the manufacturer (New England Biolabs).

2.1.4. Determination of $^{45}Ca^{2+}$ Uptake

Cells were transfected at 80% confluence in 75-cm^2 T-flasks with 20 μg of TRPV1eGFP or TRPV1εMTH plasmids. After 48 h, 5 x 10^4 cells were detached from the plastic surface by serum-free DMEM containing 1 mM EDTA and then washed two times and resuspended in medium without EDTA. Cell suspensions were incubated in serum-free DMEM containing 1 μCi/ml $^{45}Ca^{2+}$ and ligands as indicated for 15 min at 35 °C in 96-well filtration plates (Multi-Screen-DV, Millipore, Marlborough, MA). $^{45}Ca^{2+}$-uptake was terminated on ice, and samples were processed and analyzed as described [21].

2.1.5. [^{3} H]RTX Binding

48 h after transfection in 75-cm^2 T-flasks, cells were detached from the plastic surface by serum-free DMEM containing 1 mM EDTA and then washed and resuspended in 10 mM HEPES (pH7.4) buffer, containing (in mM) KCl (5), NaCl (5.8), $MgCl_2$ (2), $CaCl_2$ (0.75), glucose (12), and sucrose (137). Intact cells were incubated (10^5 cells/well) in a filtration plate with 200 pM [^{3}H]RTX for 60 min at 37 °C and then processed as described earlier [22]. Data were analyzed by computer fit to the Hill equation as noted previously [21, 23].

2.1.6. Fluorescent Confocal Microscopy

COS7, NIH 3T3, and HEK293 cells were seeded on 25-mm coverslips and transfected with 1 μg each of the plasmid constructs, cultured for 24 h post-transfection at 35 °C, then mounted in a 1-ml chamber and examined with a MRC-1024 Bio-Rad confocal microscope. To study the two- and three-dimensional distribution of fluorescent chimeric proteins, each *x-y* plane was scanned over 1 s and at 0.2-μm increments in the *z* axis mode. To label different subcellular compartments of live cells fluorescently, the ER marker eGFP-KDEL (CLONTECH) was transiently transfected in COS7 and NIH 3T3 cells or the ER tracker Blue-White vital dye was used (Molecular Probes). To label mitochondria, MitoTracker Red was employed (Molecular Probes). The dye was incubated for 30 min at a 250 nM concentration; the cells were then washed with HBSS supplemented with 1 mM $CaCl_2$ and 0.8 mM $MgCl_2$, buffered with 15 mM HEPES (pH 7.4). Labeled cells were imaged with a MRC-1024 Bio-Rad confocal system with the appropriate GFP, Rhodamine and UV excitation and emission filters. Embryonal DRG cultures seeded on 25-mm coverslips and were loaded with the MitoTracker Red probe (Molecular Probes).

2.1.7. $[Ca^{2+}]_i$ Microfluorometry

For determination of $[Ca^{2+}]_i$, cells were cultured in glass bottom dishes (MatTek Corp., Ashland, MA) and then transfected with 2 μg of TRPV1eGFP plasmid. After 24 h in culture, cells were loaded with Fura-2/AM (Molecular Probes, Eugene, OR) for 30 min at 37 °C. Single cells expressing the TRPV1eGFP construct were identified by eGFP fluorescence and were selected based on visual inspection of fluorescence intensity. In all experiments, cells exhibiting intermediate fluorescence in comparison to other cells in the same dish were picked for analysis. To determine the $[Ca^{2+}]_i$, the excitation ratio of Fura-2 at 340 and 380 nm was recorded photometrically in Krebs' buffer at a 10-Hz sampling rate and integrated over 0.5 s, as described previously [24]. $[Ca^{2+}]_i$ was calculated using the ratio based equation [25].

2.1.8. Fluorescent Ca^{2+} Imaging

Cells cultured on poly-D-lysine-coated coverslips were pre-loaded with 5 mM Indo-1 AM or Fluo-4 AM dyes. After incubation for 30 min at 34 °C, the cells were washed three times in IM to remove excess dye and examined under confocal microscope. To record in "zero" extracellular Ca^{2+} cells were washed for 1 min in IM containing 10 μM Ruthenium Red (RR) and 100 μM EGTA without the addition of any Ca^{2+}. For determination of $[Ca^{2+}]_i$, an upright microscope (Olympus BX60) illuminated with an arc lamp and equipped with a 20x UAPO/340 water immersion objective was used. A shutter (Uniblitz, Rochester, NY), an excitation filter (495 nm), appropriate dichroic mirrors, and a long pass filter (515 nm) were

positioned in the light path. The fluorescent signal was intensified (Model KS-1380, Videoscope International, Washington, D. C.) before capture by a CCD camera (Pulnix, Sunnyvale, CA). Images were digitized and integrated (2 frames/image) on a Macintosh computer running Synapse 3.7, an image acquisition and analysis program (Synergy Research, Silver Spring, MD). Neurons were outlined, and fluorescent intensities were analyzed. Fluorescence intensity values in the non-zero pixels within each slice were averaged (F) and plotted as normalized fluorescence intensities ($\delta F/F0$) against time. Analysis of the traces and area measurements was performed by the Kaleidograph software (Synergy Software, Reading, PA). The Indo-1 imaging was performed by the MRC-1024 Bio-Rad confocal system. To quantitate the fluorescence ratio, perikarya of the cells were marked with the graphic tools of the LaserSharp software in the field of a 40x objective of the Bio-Rad confocal system. Ratiometric imaging was performed at 10-s intervals with an UV laser, and the ratio of fluorescence intensity emitted at 405 and 485 was calculated.

2.2. Primary Neuronal Cultures

2.2.1. Rat DRG Culture

DRG neuron-enriched cultures were prepared from embryonic rats (E16). Briefly, embryos were removed from the uterus and placed in Petri dishes containing Lebowitz medium (Life Technologies, Inc.). The cords were dissected, and the DRGs were stripped off with the meninges. Cells were digested in 0.125% trypsin at 37 °C for 20 min. For plating, dissociated cells were changed into minimal essential medium containing 5% horse serum and 50 ng/ml nerve growth factor (NGF). Cells were seeded on 25-mm glass coverslips or on multiwell plates. Surfaces were coated with poly-D-lysine and laminin. DRG cultures were maintained in DMEM containing 20 mM HEPES, 7.5% fetal bovine serum, 7.5% horse serum, 5 mg/ml uridine supplemented with 2 mg/ml FUDR to inhibit cell division and 50 ng/ml NGF to promote neuronal survival and differentiation. Cultures were selected in this medium for 1 week, at which point well differentiated neurons and nondividing cells dominated the population. Primary DRG cultures in this stage were used for microscopy.

2.2.2. Human DRG Culture

Human DRG tissue was obtained from Advanced Bioscience Resources Inc. (Alameda, California, USA). Ganglia were collected in cold Lebowitz medium (Invitrogen Corp., Carlsbad, California, USA). After digestion with 0.125% trypsin at 37°C for 25 minutes, cells were seeded on coverslips coated with poly-D-lysine. Culture medium contained DMEM with 20 mM HEPES, 7.5% FBS, 7.5% horse serum, and 50 µg/ml nerve

growth factor. After the first day, 5 mg/ml uridine, 2 mg/ml FUDR (Sigma-Aldrich, St. Louis, Missouri, USA) was added to inhibit non-neuronal cell division.

2.3. Histology and Immunohistochemistry

2.3.1. Histology and immunohistochemistry on rat DRG neurons

Rat dorsal root ganglia were fixed in S.T.F. (Streck Laboratories, INC. Omaha, NE) for 24 hours and paraffin processed. Five μm sections were stained for H&E or used for immunohistochemistry. Primary antibodies used were anti-rat TRPV1, (1:1,000) (Affinity Bioreagents), CGRP (1:2,500) and mouse monoclonal N52 (1:2,000) (Chemicon International). In short, following deparaffinization sections were blocked with 10% normal goat serum (S-1000, Vector Laboratories, Inc., Burlingame, CA). Epitope unmasking was performed with Target Retrieval Solution (S1700, Dako, Carpinteria, CA) at 95˚C for 20 minutes. Visualization of the immunocomplexes was done by the Vectastain Elite Rabbit IgG and the Peroxidase Substrate Kits (PK-6101 and SK-4100, Vector Laboratories, Inc., CA). Control sections for assessment of non-specific binding were processed in an identical way except for omission of the primary or secondary antibodies. The stained sections were visualized with an Olympus BX 60 microscope, equipped with a CCD Camera (Diagnostic Instruments Inc. Burroughs, MI).

2.3.2. Histology and immunohistochemistry on adult human DRG

Tissue for neuroanatomical studies was obtained under a protocol with the Delaware Valley Kidney 1 Human Organ Donor Program. DRGs were removed within 1 hour of cessation of perfusion, and either specimen was paraffin-processed or frozen sections were cut for histochemistry or immunohistochemistry, respectively. Human TRPV1-specific antibody (PA1-748; Affinity BioReagents Inc.) was used at a dilution of 1:500 and incubated overnight at 4°C visualized with FITC-conjugated AffiniPure Donkey Anti-Rabbit IgG (711-095-152; Jackson ImmunoResearch Laboratories Inc., West Grove, Pennsylvania, USA) and counterstained with Hoechst 33342 dye (H3570; Molecular Probes Inc., Eugene, Oregon, USA). Control sections for assessment of nonspecific binding were processed in an identical way, except that primary antibody steps contained 2.5 μg peptide antigen/ml.

2.4. In vivo experiments

2.4.1. Animals.

Procedures for rat studies followed the NIH Guidelines for the Care and Use of Laboratory Animals, and were approved by the National Institute of Dental and Craniofacial

Research Animal Care and Use Committee. A protocol to treat dogs with RTX was approved by the University of Pennsylvania School of Veterinary Medicine Institutional Animal Care and Use Committee prior to the start of the study.

2.4.2. Intraplantar RTX injection.

Unanesthetized adult male Sprague–Dawley rats (200–400 g) were gently restrained and RTX (0.0625–10.0 μg, LC Laboratories) or vehicle (0.25% Tween 80 in phosphate buffered saline, 0.05% ascorbic acid) was injected (i.pl., 100 μl) into the mid-ventral surface of the hindpaw.

2.4.3. Trigeminal microinjection.

Male Sprague-Dawley rats (300 g, n = 54) were anesthetized with ketamine/xylazine and mounted in a stereotaxic frame. A 10-μl Hamilton syringe (Hamilton Company, Reno, Nevada, USA) was positioned at 2.5 mm posterior and 1.5 mm lateral to the bregma. The skull was drilled, and the needle was advanced until it gently touched the base of the skull; the needle was retracted 0.1 mm, and RTX (20 or 200 ng) was injected in a volume of 2 μl over 10 minutes. A pharmacological- grade preparation of RTX was formulated as follows: PBS, pH 7.2, containing 0.1 μg/μl RTX, 0.05% ascorbic acid, and 7% Tween 80. Vehicle contained no RTX. The Pharmaceutical Development Section, Clinical Center, NIH, performed characterization of this preparation.

2.4.4. Intrathecal injection of rats.

Animals (n = 58) were anesthetized with isoflurane, and RTX (10–200 ng in 30 μl over 10 minutes) or vehicle was administered by inserting a 20-gauge guide catheter into the L4/L5 interspace. A PE-10 catheter was advanced 1 cm into the intrathecal space. The criterion for the intrathecal placement was withdrawal of clear cerebrospinal fluid.

2.4.5. Sensory and physiological tests.

The afferent functions of the trigeminal nerve were tested in 30 rats after TG microinjection of RTX using the CAP-induced eye-wipe response. A stock solution of 5% CAP was made in 75% ethanol, 0.05% ascorbic acid (Sigma-Aldrich). After dilution to 0.01%, CAP with saline (50 μl) was dropped into the cornea, and eye wipes were counted for 1 minute. A separate group of seven rats was tested over the course of a year. Efferent functions of the trigeminal nerve were tested in rats (n = 7) at 7 days after injection. Rats were anesthetized with ketamine/xylazine and hair removed with Nair (Carter-Wallace Inc., New

York, New York, USA). After washing thoroughly with water, 5% CAP cream, containing 0.05% ascorbic acid, was applied evenly to the entire head and shoulder region. After 15 minutes, the left femoral vein was catheterized and a 0.5-ml bolus of Evans Blue (Sigma-Aldrich) (20 mg/kg in saline) was injected. Radiant-heat thermal testing was performed on unrestrained rats (n =58) according to previously published procedures[26, 27]. The endpoint recorded was latency (seconds) to paw withdrawal. Thermal intensity was set to produce a withdrawal latency of 8–10 seconds. A 10-second withdrawal latency corresponds to a temperature at the surface of the paw of 45.2°C [26]. Mechanical sensory stimulation included a pinch with toothed forceps, the application of graded von Frey filaments, and assessment of pinprick hyperalgesia as described previously [28]. Rats treated 3 and 10 days and 1 year (n = 4 per group) prior to mechanosensory testing and a group of untreated controls (n = 4) were examined. Reduction in inflammatory hyperalgesia was tested by radiant thermal heat 5 days after intratheal injection of either vehicle or RTX (200 ng; n = 8, four to a group). Rats were lightly anesthetized with isoflurane, and the plantar surface of the left hindpaw was injected with 100 µl 4% Carrageenan (C-3889; Sigma-Aldrich), dissolved in saline. Assessment of locomotion and proprioception was performed in the intrathecally injected (vehicle and RTX) rats on an accelerating Rota-Rod (4–40 rpm in 5 min; model 7750; Ugo Basile Biological Research Apparatus, Comerio, Italy).

2.4.6. Intrathecal injection in dogs

We recruited dogs having advanced cancer or osteoarthritis (n = 8), whose owners brought them to the veterinary clinic for evaluation because of pain not well controlled by current medications. This was an open-design study, both for ethical reasons and because of the very prolonged duration of action of a single intrathecal dose of RTX, which we hypothesized would provide sustained improvement in activity and animal personality issues, thereby outlasting a 'placebo effect' in third-party observers. Dogs were maintained under general anesthesia with isoflurane and oxygen. The cisterna magna was penetrated with a 20-gauge 4-cm spinal needle. When the needle is properly placed, the cerebrospinal fluid flows freely. A single dose of 1 µg/kg of RTX was injected over 10 minutes, followed by 0.2 ml of sterile saline; any arousing effects were controlled with intravenous fentanyl.

2.4.7. VAS ratings.

To assess the effect of a single dose of intrathecal RTX, owners were asked to rate their dogs' pain before and after treatment, using a 100-mm VAS, with zero designated as no pain and 100 the worst pain imaginable. Ratings were obtained before injection, and at 2, 6, and 10 weeks after injection. (The lack of data in several cases results from euthanasia

following progression or complication of the main pathology).

3. RESULTS

3.1. Molecular biological characterization of plasmid constructs

The vanilloid receptor belongs to the Transient Receptor Potential channel family (TRP). It has six transmembrane domains, an N-terminal portion with multiple ankyrin repeats and a C-terminal end (Fig. 1*a*). The functional channel forms tetramers with other TRPV1 molecules[29]. To be able to monitor the function of the receptor we generated C-terminally tagged mutants. For this purpose we used the ε-tag motive from the protein kinase C epsilon (PKCε) and in another construct the enhanced green fluorescent protein (eGFP) molecule. The TRPV1ε and TRPV1eGFP plasmid constructs were expressed in COS7, HEK293, and NIH 3T3 cells by transient transfections. Western blot analysis with polyclonal eGFP and ε-tag-specific antibodies demonstrated that the TRPV1eGFP and TRPV1ε-chimeric

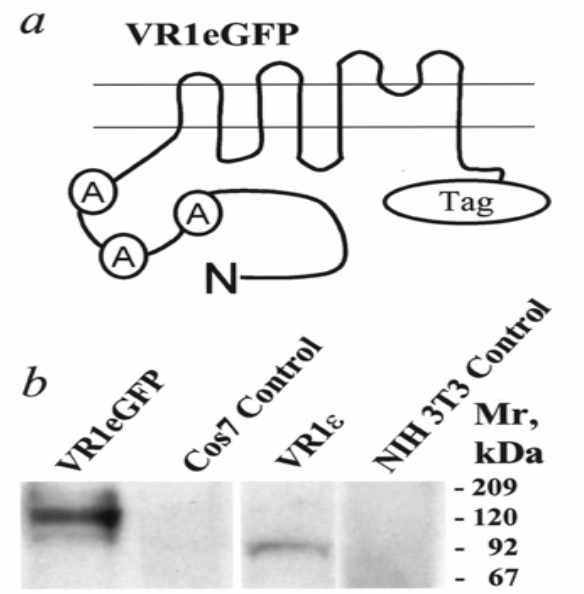

Figure 1. (*a*), schematic representation of C-terminally tagged TRPV1. (*b*), Western blot analysis of the chimeric proteins. The intracellular ankyrin repeats, the enhanced green fluorescent protein-, and ε-epitope-tagged chimera proteins are abbreviated as A, VR1eGFP, and VR1ε, respectively. *b,* TRPV1eGFP and TRPV1ε plasmids were transfected in HEK293 and NIH 3T3 cells, respectively. After 48 h 35 mg of total protein extract, prepared in SDS sample buffer, was analyzed for the eGFP (*lanes 1* and *2*) and ε-tag immunoreactivities (*lanes 3* and *4*) by Western blotting, employing eGFP and ε-tag specific antibodies, respectively.

proteins expressed in HEK293 and NIH 3T3 cells were of the appropriate sizes, 120 and 93 kDa, respectively (Fig. 1*b*, *1st* and *3rd lanes*). No tag-related immunoreactivity was found in the nontransfected host cells (Fig. 1*b*, *2nd,* and *4th lanes*). Repeated Western analyses with GFP- and ε-tag-specific antibodies showed no proteolytic cleavage of the TRPV1 chimeric proteins (data not shown). These transiently transfected plasmid constructs expressed proteins that exhibited identical molecular weights after the tag-specific antibodies were removed and the blots re-probed with the N-terminal specific TRPV1 antibody (data not shown).

3.2. Electrophysiology on the TRPV1 mutants

To study the electrophysiological properties of C-terminally eGFP-tagged TRPV1, plasmid constructs producing TRPV1eGFP and eGFP as a control were transiently expressed in HEK293 cells. Green fluorescent cells of medium fluorescence intensity were voltage-clamped, and the holding potential was adjusted to -60 mV. Capsaicin (10 μM) induced a large inward current (Fig. 2*a*). Similar currents were also evoked by administration of 125 pM

Figure 2. Vanilloid currents in transiently transfected HEK293 cells.

HEK293 cells were cultured on laminin-coated coverslips in 6-well plates and transfected with TRPV1eGFP (***a***) or eGFP plasmids (***b***). After 48 h, cells expressing the fluorescent proteins were selected for voltage clamp assays. The holding potential for all of the cells was -60 mV. *a,* 10 μM CAP was bath-perfused for 30 s for the first application and 1 min for subsequent applications to induce currents in TRPV1eGFPexpressing cells. The first treatment with CAP was shortened to reduce the amount of receptor desensitization. The antagonist 10 μM CPZ attenuated the capsaicin-induced current (*n* =4 cells). The drugs were washed out of the bath for 10 min between applications. *b,* capsaicin (10 μM) (*n*=4 cells) did not evoke currents in eGFP transfected HEK293 cells. Drug application was 1 min.

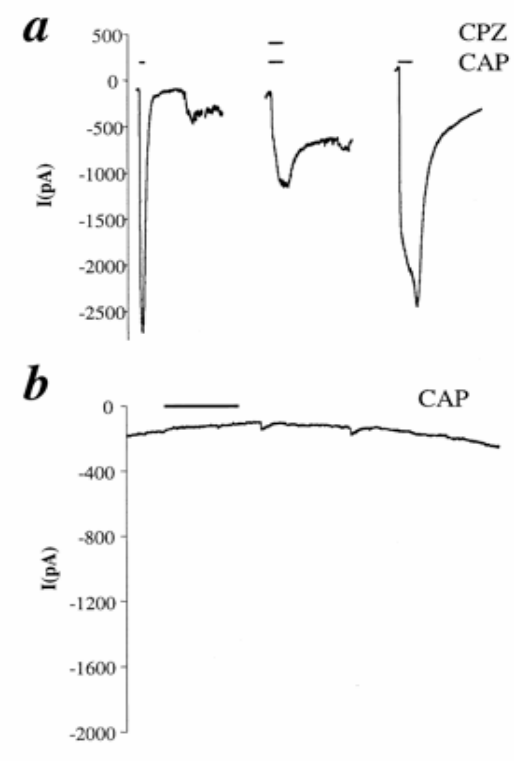

RTX to the cells; however, the currents rapidly desensitized to repeated applications (*n*=6) (data not shown). Capsaicin was noted to be less effective at inducing desensitization than RTX; therefore, CAP was used in experiments that required repeated application of vanilloid ligands (*e.g.* Fig. 2). As expected for a functional recombinant, the TRPV1eGFP-mediated current was attenuated by coincubation of an antagonist, 10 μM capsazepine (CPZ). The current *versus* voltage relationship demonstrated that the TRPV1eGFP-mediated current was not particularly voltage-sensitive. The reversal potential was near 0 mV, suggesting mixed cation selectivity for the channel (data not shown). Cells transfected with eGFP did not demonstrate currents when exposed to either CAP or RTX (Fig. 2*b* and data not shown). Likewise, non-transfected HEK293 cells did not demonstrate RTX-evoked currents. Overall, the electrophysiological properties of the eGFP-tagged TRPV1 were very similar to those described for non-tagged TRPV1 [16].

3.3. Ca^{2+}-uptake Experiments in TRPV1-eGFP and TRPV1ε-MTH Transfected Cells

In accordance with the electrophysiological data, exposure to RTX induced Ca^{2+} uptake in TRPV1eGFP-expressing HEK293 and COS7 cells. This ligand-induced Ca^{2+} influx (Fig. 3*a*) further confirms the presence of TRPV1eGFP at the plasma membrane. RTX induced $^{45}Ca^{2+}$ uptake with an ED_{50} = 100 +/- 50 pM (*n* = 3) whereas that for CAP was 0.5 +/- 0.15 μM (data not shown). Similar results were obtained for the TRPV1 tagged with the 12-amino acid ε-epitope in place of the eGFP tag. This indicates that a C-terminal tag, *per se*, does not significantly change Ca^{2+} uptake parameters. In addition, RTX-induced $^{45}Ca^{2+}$ uptake was completely blocked by 10 μM CPZ in TRPV1eGFP- (Fig. 3*a*) and TRPV1ε-expressing cells (not shown). The curves in Fig. 3*b* demonstrate the quantitative characteristics of [^{3}H]RTX binding to eGFP-tagged and ε-tagged TRPV1 expressed in COS7 cells. Both tagged recombinants exhibited a high affinity, dose-dependent interaction (*Kd* =150 +/- 10 pM, *n* = 6) and cooperativity among the receptors (Hill coefficient =1.5–2). [^{3}H]RTX binding was almost completely inhibited by co-incubation of 10 μM CPZ. No significant [^{3}H]RTX binding was detected in cells transfected with the plasmid expressing only eGFP (Fig. 3*b*).

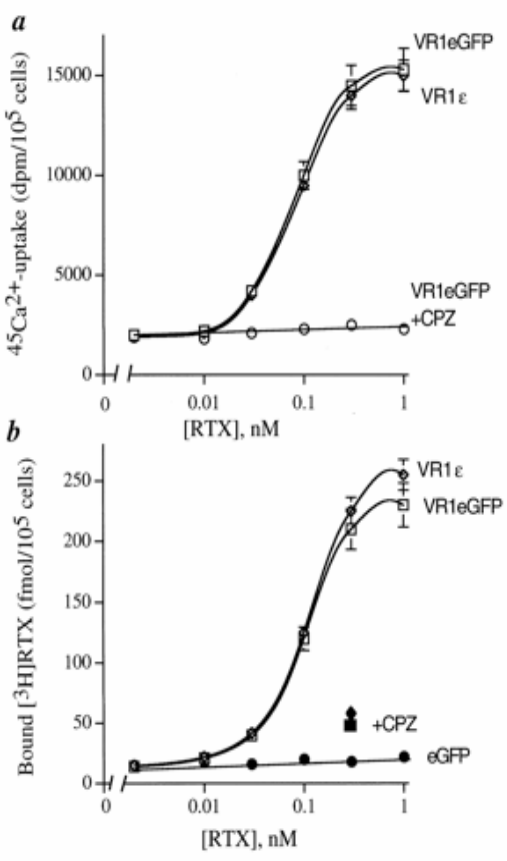

Figure 3. (***a***), RTX-induced increase of intracellular Ca^{2+} in the TRPV1eGFP (VR1eGFP *squares*) and TRPV1ε (VR1ε *diamonds*). HEK293 cells were transfected for 48 h with the plasmid constructs and then $^{45}Ca^{2+}$-uptake was induced with the indicated concentrations of RTX. The $^{45}Ca^{2+}$ uptake experiments were carried out as described above. The results were analyzed by fitting the Hill equation to the data points. The effects of 10 μM CPZ co-treatment with increasing concentrations of RTX on $^{45}Ca^{2+}$ uptake were determined with TRPV1eGFP-transfected cells (*open circles*). (***b***), demonstration of vanilloid binding activity of the TRPV1eGFP (VR1eGFP *squares*) and TRPV1ε (VR1ε *diamonds*) chimeric constructs expressed in COS7 cells. [^{3}H]RTX binding experiments were carried out 48 h following the transfection as described under. The results were analyzed by fitting the Hill equation to the data points. The effect of 10 μM CPZ on the binding of 0.5 nM [^{3}H]RTX is indicated by the *filled diamond* (VR1ε) and the *filled square* (VR1eGFP), respectively. Background binding was determined in cells transfected with a control plasmid (eGFP, *filled circles*). Results are from a single experiment carried out with triplicate determinations. Two additional experiments yielded similar results.

3.4. Confocal Imaging Data

3.4.1. Fluorescent Confocal Microscopy for the localization of TRPV1-eGFP and changes

associated with the application of RTX

Confocal fluorescence microscopy was employed to analyze the intracellular distribution of the TRPV1eGFP molecule. Optical sections taken at the plane of cell attachment to the glass surface show TRPV1eGFP fluorescence in the plasma membrane, where microvilli were labeled (Fig. 4*a*, TRPV1 accumulation also is present at the focal points in this plane, not seen with fluorescent markers of ER). Optical sections taken through the middle of the cell nucleus, disclosed TRPV1eGFP in intracellular structures consistent with the ER (Fig. 4, *b versus d*). To confirm ER localization, cells were transfected with an eGFP that was C-terminally tagged with the ER retention signal (*i.e.* the KDEL motif, Fig. 4*b*). Visualization of the transiently expressed eGFP-KDEL chimera protein in COS7 cells verified that TRPV1eGFP indeed stained the same ER compartment within the cytoplasm and around the nucleus (Fig. 4, *b versus d*). Furthermore, the same ER colocalization result was obtained when TRPV1eGFP -expressing cells were costained with the ER-tracker vital dye (Molecular Probes) (Fig. 4, *h* and *i*). Fig. 4 illustrates localization of TRPV1 in Cos7 cells, but similar ER localization was seen in HEK293 and NIH 3T3 cells, indicating, that it is not a cell type-specific anomaly. ER localization was observed over a range of transfection efficiencies, and the distribution between the plasma membrane and ER was similar in cells expressing TRPV1eGFP at different levels (not shown). The proportionality between plasma membrane and ER also was maintained in a cell line stably expressing relatively lower levels of TRPV1ε from the non-induced MTH promoter (data not shown). These data, as well as results from immunocytochemical staining of fixed DRG neurons, which show a high density of staining throughout the neuronal cytoplasm [15], suggest the distribution is not simply due to over expression. Dual wavelength imaging studies demonstrated that the intracellular compartment containing TRPV1eGFP (*green*) was distinct from the filamentous mitochondria (*red*), which were labeled by the red MitoTracker dye and are generally thicker than the ER (Fig. 4*f*). Previously it was noted that addition of ionomycin to cells induces intracellular membrane fragmentation due to permeabilization of the plasma membrane to cations [30]. This was verified in baseline control studies using the eGFP-KDEL expressing plasmid, which showed that ionomycin treatment induced membrane fragmentation of the ER (Fig. 4, *b versus c*). This fragmentation was identical to what occurred with TRPV1eGFP-expressing cells upon exposure to 1 nM RTX. In these cells a 20-s exposure induced fragmentation of the ER (Fig. 4, *d* and *e*) and, simultaneously, a rounding up of the filamentous mitochondria (Fig. 4, *f versus* g). Testing of a second vanilloid ligand, CAP (1 μM), also demonstrated membrane fragmentation with similar dynamics as noted with RTX (not shown). With the appropriate sets of fluorescence filters, we observed no mixing between the TRPV1eGFP vesicles (*green*)

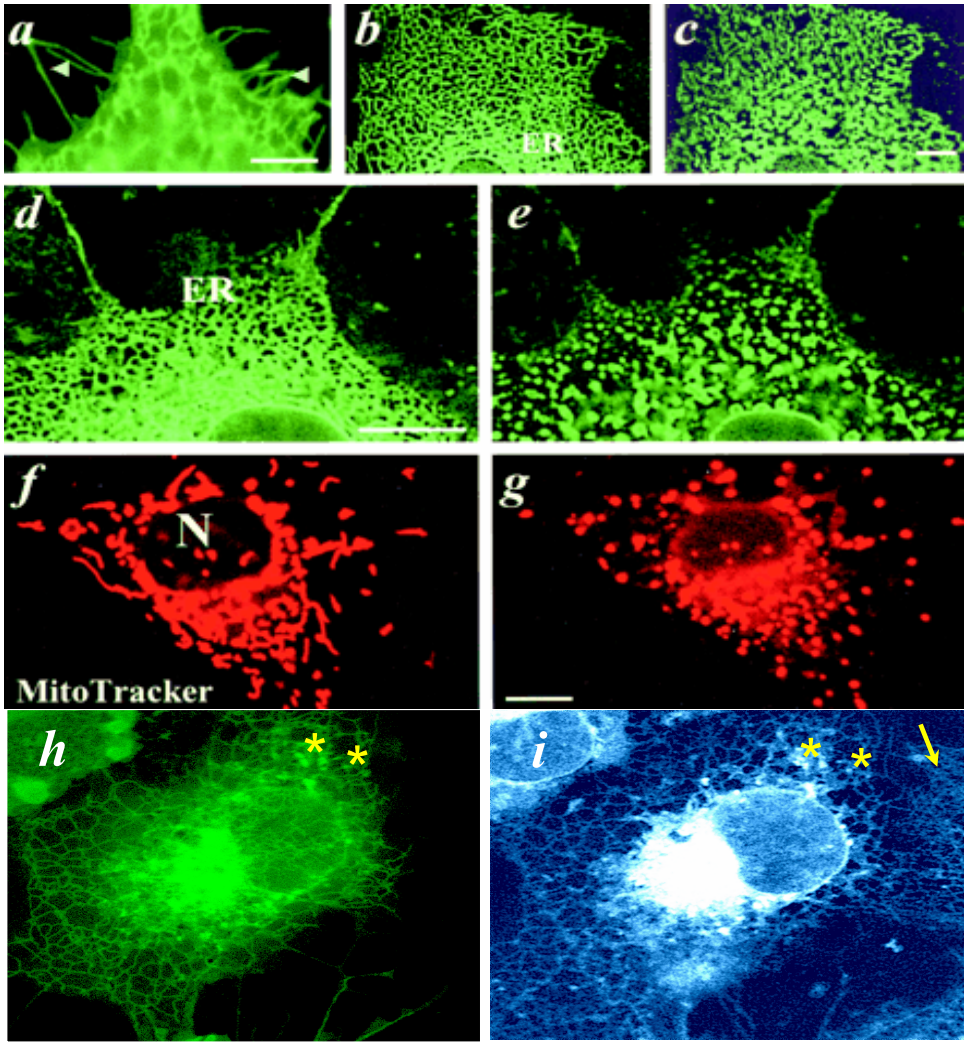

Figure 4. Localization of TRPV1 and early dynamics of TRPV1 activation imaged in live cells. To determine the *in vivo* cellular location of the fluorescently labeled TRPV1eGFP (***a***, ***d***, and ***e***), studies with eGFP-KDEL (***b*** and ***c***) and MitoTracker vital dyes (***f*** and ***g***) were carried out 24 h after transfection in COS7 cells employing laser confocal microscopy. In optical sections close to the glass surface TRPV1eGFP was localized in microvilli at the plasma membrane in transiently transfected live COS7 cells (*a*). The bright spots are the focal points at the basal membrane glass interface. *Arrowheads* show the extrusion of TRPV1eGFP-labeled plasma membrane microspikes at the edge of the cell. In median optical sections, at level of the cell nucleus, TRPV1eGFPs are depicted in an intracellular membrane network similar to ER (*d*). Similarities in eGFP-KDEL and TRPV1eGFP in this optical section verify that TRPV1 indeed can localize to the ER compartment. To study the effects of ionomycin (4-bromo-A23187) on intracellular membranes, the same cell was imaged by the expressed ER marker, eGFP-KDEL (*b* and *c*) before and 10 s after addition of 4 μM ionophore. The effects of RTX treatment were depicted with the TRPV1eGFP (*d* and *e*) and MitoTracker (*f* and *g*)-derived fluorescence before and 20 s after addition of 1 nM RTX. The membrane permeabilization to cation by ionomycin or activation of TRPV1 by RTX resulted in a similar ER vesiculation (*c* and *e*), indicative of similar mechanism and vesiculation of the mitochondria (*g*) *bar,* 5 μm. (***h*** and ***i***) Live cell imaging (single confocal section) on a TRPV1-eGFP transfected Cos7 cell. TRPV1-eGFP localizes to the ER, Golgi and the plasma membrane. The ER-Tracker Blue-White shows identical ER distribution (asterisks denotes identical spots on the ER, the arrow points to a non-transfected cell).

and the mitochondrial membranes (*red*) (data not shown). In cells expressing only eGFP, the structure of the mitochondria and ER did not change upon exposure to vanilloids, indicating the dependence for these effects on the presence of the TRPV1 receptor. Thus, within the first

few seconds after vanilloid exposure, coincident and structurally similar intracellular organelle remodeling occurs for both the ER and the mitochondria.

3.4.2. RTX induces increase of intracellular Ca^{2+} in TRPV1-eGFP transfected cells

The effect of RTX on cytosolic Ca^{2+} was studied by microfluorometry in transfected cells loaded with the Ca^{2+}-sensitive dye, Fura-2 AM. The resting intracellular calcium concentration ($[Ca^{2+}]_i$) was similar (~50 nM) in COS7 cells transfected with either TRPV1eGFP or eGFP plasmids. Addition of 1 nM RTX induced a rapid (within 10 s) elevation of $[Ca^{2+}]_i$ in TRPV1eGFP-expressing cells which peaked at 500 nM at ~1 min (n= 3) and, consistent with the concurrent ER and mitochondrial damage (Fig. 4, *e* and *g*), and did not return to resting levels (Fig. 5*a*).

3.4.3. Extended confocal imaging on TRPV1eGFP expressing COS7 cells after addition of RTX

The preceding experiments focused on events occurring within the first few seconds following exposure to TRPV1 agonists. To extend the time of cellular observation, serial 1-s confocal microscopy scans were performed at 1-min intervals on live TRPV1eGFP-expressing cells. In these experiments the early events occurred as described Fig. 5*a* and *b* (*e.g.* transmembrane Ca^{2+} flux, intracellular remodeling, within 30 s in 13 out of 15 cells). Within 3 min after RTX administration, the nuclear membrane was outlined with TRPV1eGFP fluorescence, and ER membrane vesicles were observed around the nucleus (Fig. 5*c*). Then, progressively growing blebs were noted in the nuclear membrane (2 out of 10 at 5 min and 9 out of 10 cells at 10 min). In the cell shown, the membrane degradation concluded with bursting of the plasma membrane at 43 min (Fig. 5*c*). Other cells displayed similar nuclear changes and cell disruption within 1–2 h (3 out of 5 within 1 h and 5 out of 5 monitored for 2 h in one experiment). Lower doses of RTX (<0.1 nM) evoked slower nuclear membrane fragmentation, but eventually resulted in cell lysis (4 out of 4 cells within 3 h). The effects were not due to the repetitive scanning, since single scans of transfected cells performed at 30 min after RTX administration also revealed (8 out of 8) identical effects of RTX on intracellular membrane structures. Figure 6 summarizes quantitatively the fluorescence scanning confocal microscopy data collected in repeated experiments. ER fragmentation was noted in 16 cells within 6 s of adding 1 nM RTX; vesiculation was

Figure 5. Ca^{2+} microfluorometry and cell death.

For microfluorometry of intracellular free Ca^{2+} (***a***), TRPV1eGFP-expressing COS7 cells were cultured and transfected in glass bottom dishes and then loaded with the

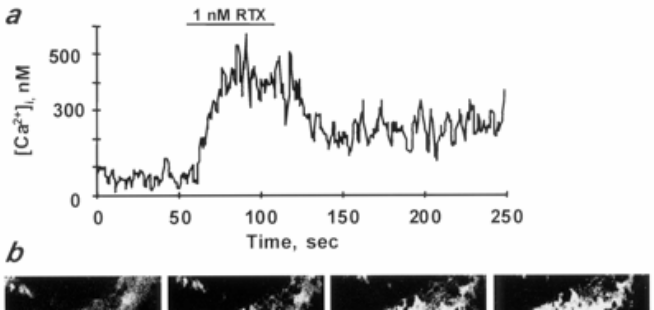

Ca^{2+} indicator dye Fura2/AM for 30 min. Single TRPV1eGFPtransfected cells were first identified by their green fluorescence. Once the cell was in focus, microfluorometric determinations of $[Ca^{2+}]_i$ were carried out for 60 s and then 1 nM RTX was perfused for 1 min as indicated. To reduce the noise of single cell recordings 5 consecutive data points were averaged. (***b***), live cell imaging of short term membrane remodeling due to RTX treatment were carried out in COS7 cells expressing TRPV1eGFP. RTX (1 nM) was added 24 h after transient transfection, and selected cells were scanned for 1 s at 30-s intervals as indicated. Remodeling of the ER started within 30 s, coincident with the rise of $[Ca^{2+}]_i$. (***c***), for long term *in vivo* monitoring of RTX effects, cells were continuously perfused in an imaging chamber for 1 h. Following 3 min of perfusion, a representative TRPV1eGFP-expressing cell was selected and imaged by 1-s laser scanning at 1-min intervals for 45 min. Nuclear blebs became apparent within 3 min, and cell lysis occurred 43 min after the RTX was administered. Other cells displayed similar loss of integrity, and the data are summarized graphically in Figure 6.

completed within 1 min in each cell monitored (scans were done every 6 s, n=30). ER vesiculation directly corresponded to the time course determined for RTX induced $[Ca^{2+}]_i$ accumulation (Fig. 5*a*). The first nuclear bleb appeared 2 min after RTX treatment (2 out of 30) and then each observed cell (n=30) showed at least 1 bleb by 10 min. Cell lysis started as early as 10 min after RTX addition (1 out of 30 cells) and was complete within 2 h (30 out of 30 cells).

3.4.4. Conformational changes of mitochondria in rat DRG neurons after RTX treatment

The mitochondrial changes coincided with the ER remodeling and can be used to indicate the effect of vanilloids in sensitive cells (Fig. 4, *f* and *g*). To verify that the rapid intracellular membrane changes observed in heterologous cells expressing TRPV1 also occurred in small-size DRG neurons, experiments were carried out on primary cultures from rat DRGs (Fig. 7). Cultures were preincubated with the red MitoTracker dye and then exposed to 1 nM RTX. Small size neurons were selected and monitored by confocal microscopy employing 1-s scans before and after treatment with vanilloids. Neurons in this size range were previously determined to be TRPV1-positive with an antibody raised against the N- terminal 18 amino acids of TRPV1 (data not shown). The MitoTracker dye revealed normal, slightly elongated

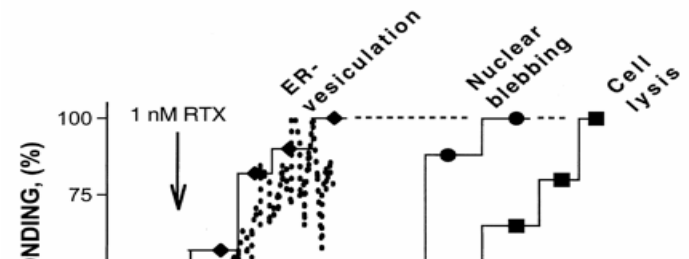

Figure 6. Quantitative analysis of membrane changes due to 1 nM RTX treatment depicted by confocal microscopy. Imaging data were derived from 30 independent transient transfection experiments carried out with TRPV1eGFP-expressing COS7 cells; cells exhibiting an intermediate level of fluorescence were chosen for imaging. *Symbols* at each step of the three graphs represent the percentage of cells from the 30 cells imaged responding within the time frames indicated (*e.g.* the *1st diamond* indicates that 16 cells responded with ER vesiculation within 1–6 s). The *dotted line* superimposed on the graphs represents the smoothed accumulation curve of $[Ca^{2+}]_i$ from Figure 5. The entire tubular ER network, decorated with TRPV1eGFP previous to 1 nM RTX treatment, changed into circular ER vesicles (*diamonds*); the first nuclear blebs were observed at 2 min (*circles*). Loss of cell membrane integrity was seen in 1 cell out of 30 at 10 min and progressed until lysis of all 30 cells was complete at 2 h (*squares*).

mitochondria in untreated small size DRG neurons (Fig. 7*a*). Treatment with RTX induced the mitochondria to change conformation within 20 s (Fig. 7*b*), similar to the ER membrane

Figure 7. Live confocal imaging of MitoTracker dye stained, small sized DRG neurons. (***a***), Small diameter DRG neuron before and (***b***) after 1 nM RTX treatment. Mitochondria of a glial cell are shown from the same culture 10 min after the RTX treatment (***c***). In the spherical neuronal perikarya, the otherwise elongated mitochondria are packed densely (*a*), but the fragmentation due to RTX is evident (*b*), especially when compared with well preserved mitochondria, depicted in the large, flat glial cell from the same culture (*c*). The glial cell shown is typical; none of the glia in the culture were affected by RTX. *Scale bar,* 2 μm.

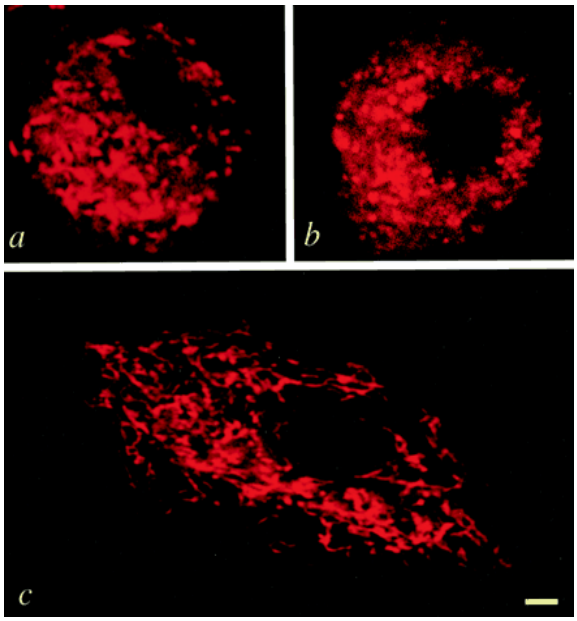

and mitochondrial kinetics observed in COS7 cells ectopically expressingTRPV1eGFP (Fig.4, *d* and *f versus e* and *g*). RTX at 1 nM concentration was without effect on mitochondria localized in the glial cell population (Fig. 7*c*) or in nearby large neurons within the field of view (data not shown).

3.4.5. Extended confocal imaging on rat DRG neurons after addition of RTX

The above experiments demonstrated that vanilloids rapidly target the ER and mitochondria at the cell body in small size DRG neurons expressing TRPV1, producing effects within seconds. To address the end point of the RTX associated cellular changes, DRG neuron cultures were subjected to longer exposure of RTX. Dual wavelength fluorescent imaging was employed. The change in $[Ca^{2+}]_i$ was monitored by Indo-1 AM, a calcium sensitive dye, and incapacitated neurons were depicted by increase of nuclear staining by propidium iodide (PI). In repeated experiments, vanilloid specific neurons in the field of view demonstrated instant increases in $[Ca^{2+}]_i$ (within seconds) upon administration of 25 nM RTX. Neurons exhibiting the RTX- induced increase in $[Ca^{2+}]_i$ started to accumulate PI in the nucleus ~40 min after addition of RTX; a time that coincides with loss of plasma membrane integrity in TRPV1eGFP-expressing COS7 cells exposed to RTX (Fig. 5). In the same microscopic field there were neurons that neither responded to RTX with an elevation in $[Ca^{2+}]_i$ nor accumulated PI even after 2 h of RTX exposure (Fig. 8). This result was consistent with the idea that these neurons do not express TRPV1 and reinforced the cellular and molecular specificity of vanilloid actions on DRG neurons. Repeated time course observations with DRG cultures indicated similar dynamics for DRG neuronal death as described for transiently (see Fig. 6) or stably transfected NIH 3T3 cells (not shown) expressing recombinant TRPV1. Elevated $[Ca^{2+}]_i$ can induce cytotoxicity within minutes to hours in TRPV1-expressing cells or specific DRG neurons, as demonstrated in previous experiments. This suggests that vanilloid application to the perikarya may be an effective means for specific deletion of nociceptive neurons.

3.4.6. Functional characterization of $TRPV1_{ER}$

Calcium-imaging experiments were performed on native non-transfected rat DRG neurons. Because the DRG culture is a heterogeneous population of neurons, a scouting or screening pulse of capsaicin (1 μM CAP in 1.25 mM Ca^{2+} for 15 s) was administered to identify TRPV1-positive neurons and the short application time allowed us to minimize any desensitizing effects of CAP (data not shown). To functionally characterize the ER-dependent elevations of $[Ca^{2+}]_i$ in isolation, experiments were carried out in a closed flow- through chamber using buffer containing 10 μM Ruthenium red (RR), a PM-impermeable TRPV1 channel blocker, and 100 μM EGTA to ensure extracellular Ca^{2+} levels of 10^{-7} M (zero $[Ca^{2+}]_o$). RR effectively blocks Ca^{2+} entry through TRPV1 in radioactive calcium transport experiments (data not shown) [31]. Once the CAP-sensitive neurons were identified, the perfusion medium was changed to zero $[Ca^{2+}]_o$ containing 10 μM RR. In the absence of

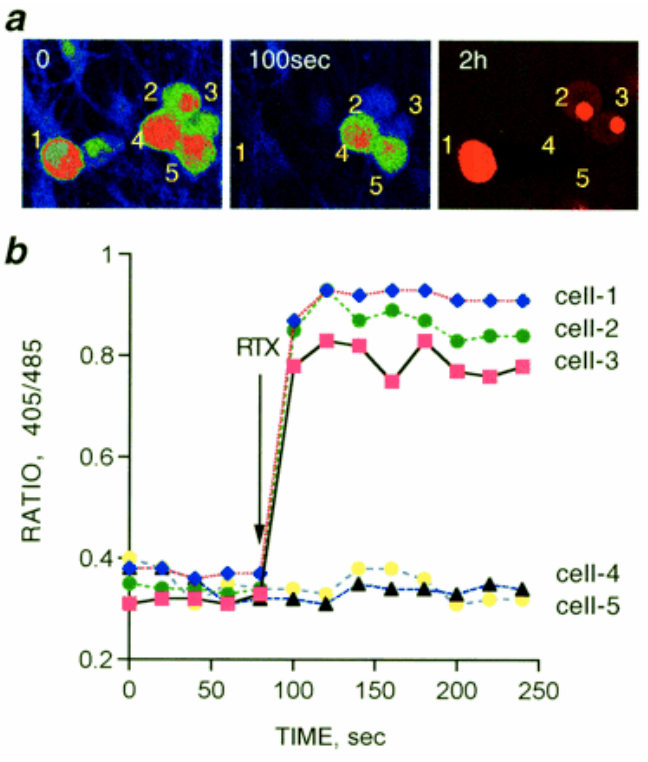

Figure 8. Relationship between RTX-induced accumulation of $[Ca^{2+}]_i$ and cell death in DRG neurons. Cells were examined by confocal microscopy at 405 and 485 nm. Individual cells are numbered in (***a***) and ratios of 405/485 of the numbered neurons are plotted in (***b***). Dissociated DRG neurons were seeded on poly-D-lysine pre-coated coverslips. Cultures were loaded with the Indo-1 AM, 30 min before the experiments, and then washed and changed into recording medium containing 1 mM $CaCl_2$. PI was added just before confocal microscopy (40x objective). First, ratio imaging at 405 and 485 nm was carried out. Frames taken on the 485 nm channel are shown, employing a geographic look-up table (*a*, 0 and 100 s). PI fluorescence was depicted on the red channel at 2 h, as indicated. RTX (25 nM), added at 70 s, induced an instant change in the 405/485 ratio as illustrated visually by the denominator channel (*a*, 0 and 100 s), and plotted in *b*. In some neurons (*cell-1, -2,* and *-3*) the *red* color shifted in the *blue* direction, indicative of a steep elevation in $[Ca^{2+}]_i$ (within seconds). In other cells (*cell-4* and *-5*) little change in color (*red*) indicated a steady, low basal level of $[Ca^{2+}]_i$. The identical cells that reacted to RTX with an elevated $[Ca^{2+}]_i$ also accumulated PI in the nucleus (*cell-1, -2,* and *-3*), indicating plasma membrane damage (*a*). Neurons resistant to RTX-induced elevation of $[Ca^{2+}]_i$ excluded PI even after 2 h (*cell-4* and *-5*). Similar results were recorded in two additional DRG cultures.

extracellular calcium and with the $TRPV1_{PM}$ channel blocker RR, RTX (1.6 μM) produced almost complete depletion of the TRPV1-sensitive pool (Fig. 9*a*) because no release from the ER pool is evoked by a second RTX application. This observation suggests that RTX extends the open state of the TRPV1 channel to the point where, in zero $[Ca^{2+}]_o$, equilibrium may be reached among $[Ca^{2+}]$ in the ER, the cytoplasmic compartment, and the extracellular fluid because RTX also keeps $TRPV1_{PM}$ in the open state. In this condition, response in zero $[Ca^{2+}]_o$ does return to the basal state (Fig. 9*a*), supporting the idea that calcium either leaves the cell or is sequestered in intracellular stores such as the mitochondria. To ensure that the Ca^{2+} was released from the ER compartment after the application of RTX thapsigargin (TG) the sarco-endoplasmic reticulum Ca^{2+} ATP-ase inhibitor was added to the system. Two main neuronal populations were distinguished by their characteristic responses. The first group and the main one studied is composed of CAP-inducible TRPV1-positive neurons in which RTX elicits a strong $[Ca^{2+}]_i$ transient. In these neurons, subsequent TG exposure minimally or did not provoke further Ca^{2+} release (Fig. 9*b*). A second group of neurons did not respond to either CAP or RTX but only to TG (data not shown) and was apparently TRPV1-negative [31].

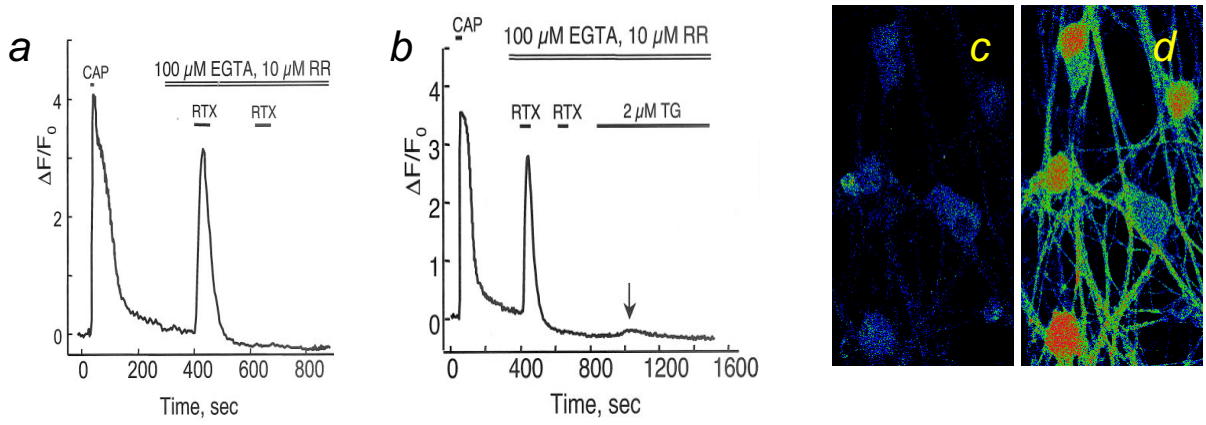

Figure 9. Evidence of overlap between vanilloid and thapsigargin-sensitive stores. (***a***), vanilloid receptor-positive cells were identified by an initial CAP treatment (1 μM, 15 s) to distinguish neurons specifically activated by vanilloids. Depletion of $TRPV1_{ER}$ store was achieved by application of 1.6 μM RTX in zero $[Ca^{2+}]_o$ (100 μM EGTA, 10 μM RR). Only the first RTX application led to an increase in $[Ca^{2+}]_i$. The second administration of RTX did not produce a change in free $[Ca^{2+}]_i$ levels. (***b***), CAP-sensitive neurons showed an increase in $[Ca^{2+}]_i$ only for the first RTX (1.6 μM) application in $[Ca^{2+}]_o$. Subsequent application of TG elicited little change (*arrow*). (***c***) and (***d***), RTX treatment elevates intracellular free Ca^{2+} in zero $[Ca^{2+}]_o$ in the neuronal processes: baseline (*c*) compared with stimulated condition (*d*). In the culture conditions used, both dendritic and axonal processes were present and both displayed an increase in $[Ca^{2+}]_i$. Traces represent separate experiments.

These findings indicate that vanilloids via $TRPV1_{ER}$ can deplete an intracellular Ca^{2+} store, which is overlapping with the TG depletable store. Vanilloid-insensitive neurons and glia responded only to TG, indicating that RTX specifically affects a subpopulation of neurons, which are presumed to be nociceptors (data not shown) [31]. The increase in Fluo-4 AM fluorescence, indicative of increased $[Ca^{2+}]_i$, was not confined to the cell body but also was observed along all of the visible neuronal processes (Fig. 9, *c* and *d*), thus revealing vanilloid-inducible $TRPV1_{ER}$-operated Ca^{2+} store throughout the entire extent of the neuronal dendritic and axonal specializations.

3.5. In vivo experimental data: peripheral application of RTX

3.5.1. Introduction to in-vivo studies

The above cellular and molecular studies suggested a novel approach for therapeutic intervention in patients with intractable pain problems. Experiments with the TRPV1 expressing cell lines showed that vanilloid-sensitive cells respond to RTX application with sustained elevation of intracellular Ca^{2+} followed by cell death. There was no effect on the parental cell lines. By exploiting the specific expression of TRPV1 in nociceptive neurons and their selective susceptibility to vanilloid agonists especially the ultrapotent RTX, in

culture conditions it was possible to eliminate TRPV1 positive primary neurons yet leave other somatosensory neurons intact. These data provided a mechanistic rationale for therapeutic intervention in which application of RTX in the vicinity of DRG or TG neuronal cell bodies in vivo would delete TRPV1+ neurons, thereby eliminating sensitivity to nociceptive input associated with inflammation, hyperalgesia, and cancer-related pain. It was further hypothesized that other sensory modalities mediated by neurons not expressing TRPV1 would remain unaffected (e.g., proprioception and high-threshold mechanosensation). We reasoned that the same mechanism applied to nociceptive nerve terminals in the periphery would reversibly inhibit pain transduction, but spare neuronal perikarya in the DRG, which are remote from the site of RTX application.

The most important aspect of every translational work (cellular to animals to humans) is whether the proposed therapy is safe and effective. Application of vanilloids directly into or around sensory ganglia is challenging for at least two reasons: a) the effect of RTX on these cellular structures have not been elucidated with thorough histopathological and immunohistochemical evaluation and b) the inherent risk of the procedure. To explore these areas we designed three strategies for pain modulation based on differential application of RTX: peripheral nerve terminal, single intraganglionic and multiganglionic (intrathecal). We employed robust, well-characterized nociceptive experimental models in rats, as well as a canine veterinary model presenting with naturally occurring conditions (cancer, osteoarthritis) that have direct relevance to humans.

3.5.2. Peripheral injection: behavioral and edema observations

Different concentrations of RTX (100 µl) were injected into the paw (mid-ventral surface) of unanesthetized adult male Sprague–Dawley rats. Following RTX injection, the animals appeared somnolent and sedated, however, they behaved normally when placed in an open field or when aroused. The degree of sedation was dose-related in both intensity and duration, with maximum effects occurring at the higher doses lasting up to 90 minutes. Low doses of RTX (0.0625 µg) had minimal sedating effects (Table 1.).

Ipsilateral injected and contralateral uninjected paw thickness (mm) was measured at the mid-central portion of the paw pre- and post-RTX injection to assess edematous changes. RTX did not induce edema at the injection site, as changes in the paw diameter were not significantly different for RTX-injected versus vehicle-injected paws and when comparing baseline values with values measured 24 h following drug administration within the same treatment groups (data not shown).

3.5.3. RTX-induced acute algesia

All doses (0.0625–0.4 μg) of RTX produced equal intensity guarding behavior and paw licking within 1–25 min following injection. However, the duration of the guarding was inversely related to dose, with low doses producing longer guarding times (Table 1).

Table 1
RTX produces general behavioral changes in a dose-related manner

	Dosage of RTX (in μg)		
	0.0625	0.125	0.25
Guarding intensity (0 = none, 1 = mild, 2 = strong)	1.2 ± 0.8	2.0 ± 0.0	1.3 ± 0.8
Guarding duration (min)	>40	<40	<10
Sedation level	Low	Moderate	High

Acute thermal testing in the first 15 min following RTX injection (0.0625–0.4 μg) demonstrated a significant reduction in paw withdrawal latency following heat stimulus (Fig. 10*a*), when compared with the baseline ($P<0.001$, two-way RM ANOVA). The transition from hyperalgesia to analgesia occurred within 2.5 h in the majority of animals at all doses, and all animals became analgesic to heat by 24 h. RTX induced c-Fos expression is blocked by peripheral local anesthetic infiltration. Upon acute injection of RTX into the hindpaw there was a significant increase ($P <0.001$, two way ANOVA) in the number of spinal lamina I cell nuclei positively stained for c-Fos (Fig. 10, *b* and *c*) in the cord ipsilateral to the injection. This comparison was made versus a vehicle injection group (Fig. 10*d*) and versus the contralateral side that was not injected (Fig. 10*b*). This c-Fos induction was significantly reduced when a local anesthetic (0.5% bupivacaine, 100 μl, intraplantar) was injected 10 min prior to RTX injection (Fig. 10, *c* and *f*). The reduction in this molecular endpoint corresponds with behavioral observations, as guarding behavior was also eliminated with bupivacaine pretreatment. We also examined lidocaine (2%) pretreatment and this was substantially less effective in blocking the acute RTX-induced guarding behavior than bupivacaine pretreatment (data not shown).

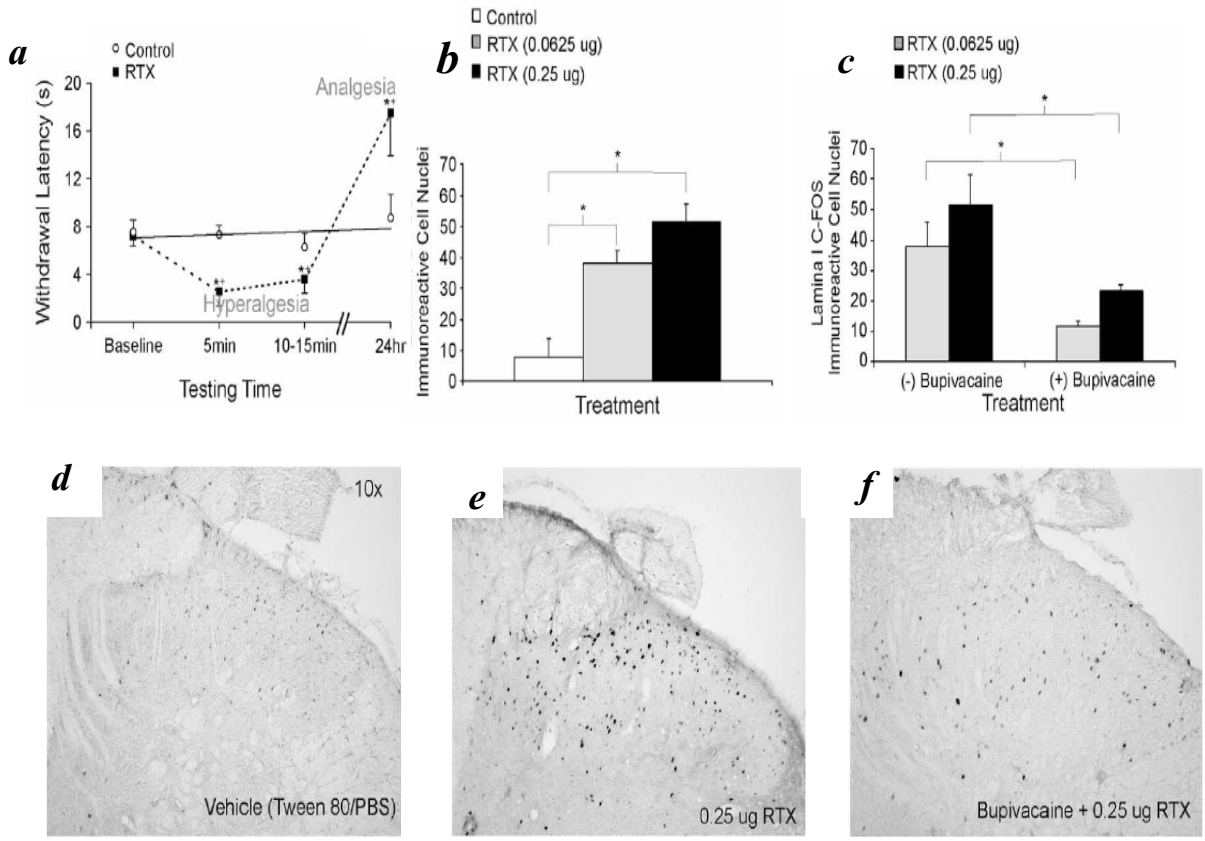

Figure 10. Peripheral administration of RTX into the hindpaw produces acute heat hyperalgesia and subsequent analgesia with associated induction of c-Fos in spinal lamina I neurons. (***a***) Hindpaw withdrawal time (s) following exposure to radiant heat source is significantly shorter (*P<0.001) on the RTX-injected side in the acute phase (#15 min) and significantly longer (*P<0.001) at 24 h when compared with the uninjected contralateral side (note that there was no significant statistical difference between responses for animals receiving 0.0625, 0.4, or 2.0 µg of RTX, therefore data were pooled, n=5). Two-way RM ANOVA with Tukey post-hoc analysis revealed a significant interaction between treatments (RTX and none) versus testing time with significantly different (*P<0.001) latency for each test time when compared with the baseline value. RTX (***b*** and ***e***) produces a significant increase (*P<0.001, one-way ANOVA and Tukey post-hoc analysis) in the number of c-Fos immunoreactive cell nuclei within spinal lamina I when compared with the vehicle (0.25% Tween-80 in PBS, 0.05% ascorbate) (***d***). This increase was significantly reduced (*P<0.001, Student's t test) when bupivacaine (***c*** and ***f***) was administered (10 min) prior to RTX injection. Bright-field micrographs (***d***–***f***) were obtained from 20 µm thick slices taken at the lumbar 4 (L4) and 5 (L5) regions and visualized using a nickel–DAB substrate and the number of c-Fos immunoreactive cell nuclei was determined at 100X magnification. Note in (*a*), a maximum latency of 20 s was used in the initial dose–response study, but several animals showed signs of tissue damage, therefore a maximum of 16 s was used for the subsequent groups.

3.5.4. RTX-induced analgesia after peripheral injection

Maximum effects from RTX were achieved at all doses (0.0625-10 µg). A significant increase of up to 3 weeks was observed in hindpaw withdrawal latency for each dose when compared with baseline levels and with the uninjected contralateral side (Fig. 11*a*). There was no statistically significant difference as compared with the lower doses when evaluating dose versus time interactions. Since the injection was remote from the cell body, it was predicted that the effect would be transient, and that TRPV1+ cells would remain intact. Histological

Figure 11. Peripheral RTX attenuates thermal nociception
(***a***) Peripheral left hindpaw (LHP) administration of 100 ng RTX yields unilateral and reversible (about 20 days) thermal analgesia (*ANOVA with Scheffe's post hoc test; $P < 0.005$) ($n = 5$ per group). RHP, right hindpaw; FP, forepaw. Retention of TRPV1-IR neurons (arrows) in L5 DRGs from RTX-injected (***b***) and noninjected (***c***) hindpaws. Cell counts of TRPV1-IR perikarya showed no significant alteration between left and right lumbar ganglia. Bars: 100 μm.

and immunohistochemical studies on ipsi- and contralateral L5 dorsal root ganglia of treated and control animals confirmed our hypothesis (Fig. 11, *b* and *c*). Counts of TRPV1-IR neurons from eight sections of L5 ganglia showed 119 ± 23 neurons on the injected side and 113 ± 10 on the contralateral side.

3.5.5. RTX specificity

Anatomical and physiological effects were regionally specific to ipsilaterally RTX-treated hindpaws. There were no statistical differences between vehicle and the RTX groups for forepaw heat withdrawal latency (Fig. 11 *a*), even in the presence of heat analgesia for the RTX-injected hindpaw. Rota-Rod results demonstrate that animals did not exhibit motor impairment following RTX injection, as the period of time (s) the animals remained on the

Figure 12. The selective nature of peripherally administered RTX. There was no evidence of RTX effect on axons of large diameter neurons or on central nervous system neurons. RTX (0.25 μg) treated animals did not differ significantly from vehicle-treated animals in Rota-Rod performance acutely (baseline, 30 min) or at longer periods (7 days). Even in the presence of sedation, motor impairment was not noted.

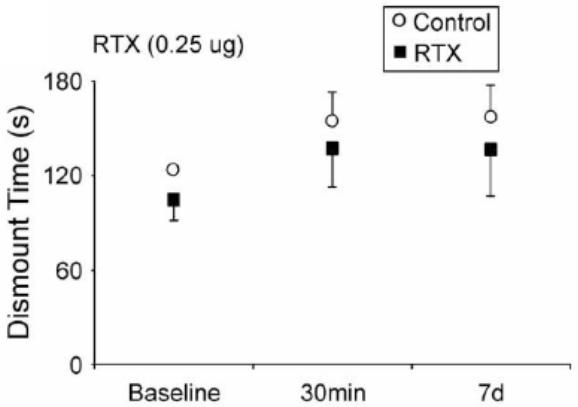

Rota-Rod was nearly identical for RTX and vehicle-treated animals (Fig. 12). The lack of motor impairment was noted at 2.5 h and 1 week following RTX administration. There were no significant differences in response to mechanical stimuli and development of mechanical hyperalgesia or analgesia was not observed following RTX injection (data not shown). There appears to be a slight decrease in mechanical sensitivity at the early time point (2.5 h), and then a slight increase over the testing period. A similar increase in sensitivity was noted on the contralateral control side over time, however, these changes were not statistically

significant when compared with either baseline values or when compared from side to side (i.e. treated vs. nontreated). Assessment of the effects on spinal reflexes demonstrated that latency (s) for tail withdrawal following tail immersion in hot (52–54 ^{o}C) water did not differ significantly among the RTX-treated groups (0.0625–0.25 μg) when compared with the vehicle-treated groups (data not shown).

3.5.6. RTX eliminates inflammation-induced heat hyperalgesia

Carrageenan-induced inflammation was produced 4 days and 1 week after intraplantar injection of either vehicle or RTX. Data for the 4 day pretreated and 1 week pretreated groups were similar. In vehicle-treated rats, carrageenan inflammation produced a significant

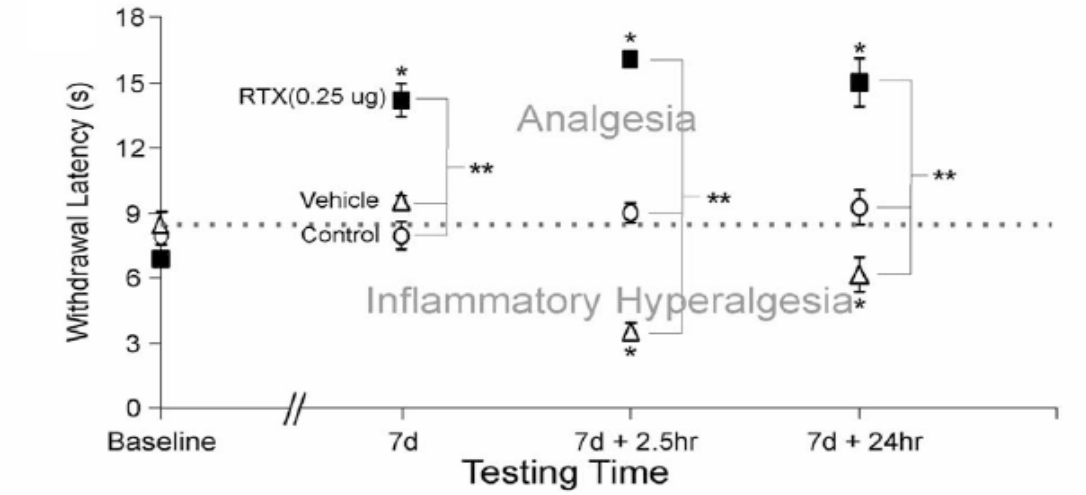

Figure 13. Treatment with RTX produced preemptive analgesia relating to the development of heat hyperalgesia pain associated with inflammation.
Significant increase in latency was produced following RTX injection at all testing points when compared with the baseline (*P<0.001) and when compared with the vehicle and contralateral sides (**P<0.001, two-way RM ANOVA with Tukey post-hoc analysis). This effect was significant even in the presence of severe inflammation. Vehicle-injected paws demonstrated a statistically significant (*P<0.001) decrease in withdrawal latency when compared with the baseline (two-way RM ANOVA with Tukey post-hoc analysis) following carrageenan (6 mg, 150 ml in PBS) injection.

reduction in the heat withdrawal latency when tested at 2.5 and 24 h (Fig. 13). There was a corresponding significant carrageenan-induced increase (P<0.001) in the number of lamina I c-Fos immunoreactive cell nuclei (Fig. 14).

The inflammatory hyperalgesia was completely prevented when animals were pretreated 1 week prior with RTX (Fig. 13). Despite the presence of inflammation, the RTX pretreated animals maintained heat analgesia, as seen by a significantly longer withdrawal latency when compared with both baseline and control (contralateral uninjected and vehicle-injected) hindpaws (P<0.001). In the RTX-treated rats, there were significantly fewer (P<0.001) lamina I c-Fos immunoreactive cell nuclei (Fig. 14) at both 2.5 and 24 h time

Figure 14. Pre-treatment with RTX produced reduction in the number of c-Fos positive nuclei in the heat hyperalgesia pain model associated with inflammation. Reduction in the number of c-Fos positive nuclei in both lamina I and V was noted in the RTX-treated animals following inflammation at both 2.5 and 24 h when compared with vehicle-treated animals (*P< 0,001, Student's t test). Cell counts were obtained from c-Fos immunostained bright-field micrographs of 20 μm thick slices taken at the lumbar 4 (L4) and 5 (L5) regions.

points after carrageenan injection, when compared with vehicle pretreated animals. The RTX-treated side did not differ from the contralateral, non-injected control side.

3.5.7. RTX reversibly eliminates immunopositive nerve staining at the site of injection

Peripheral (intraplantar) application of RTX elicited a robust, but reversible analgesic effect as tested in the radiant heat and carrageenan-induced inflammatory hyperalgesia models. The effect lasted for approximately 3 weeks, and there was no evidence of reduction of TRPV1 immunopositive cells in the L4-L5 dorsal root ganglia. The behavioral data implied structural changes affecting nerve fibers. Vehicle-injected hindpaws demonstrated normal nerve ending staining (Fig. 15*a*). Peripheral nerve fiber endings were eliminated in the area of RTX (0.1–1.0 μg) injection (Fig. 15, *b* and *c*) as quickly as 1 day post-injection. Evidence of nerve degeneration (Wallerian-like) is noted as discrete vesicles in tissue treated with RTX (Fig. 15*d*) while normal nerve architecture is noted in vehicle-treated tissue (Fig. 15*e*). By 4 weeks following injection, there was a return of the nerve bundles and endings (Fig. 15, *f* and *g*). Hematoxylin counter staining demonstrated that no cellular destruction or connective tissue changes occurred at these concentrations of RTX when injected into the hindpaw.

The peripheral injection studies showed great efficacy and also reversibility of the treatment. The observed pathophysiological effects were due to transient nerve fiber deactivation, which morphologically correlated with destruction of small diameter nerve fibers. Large diameter, myelinated fibers remained intact as it was evident in experiments using the accelerating Rota-Rod. Large and small diameter neuronal cell bodies were not affected. The effect of the peripheral injection was reversible and correlated with regeneration of the peripheral nerve endings (Figs. 11, *a*; 15, *f* and *g*).

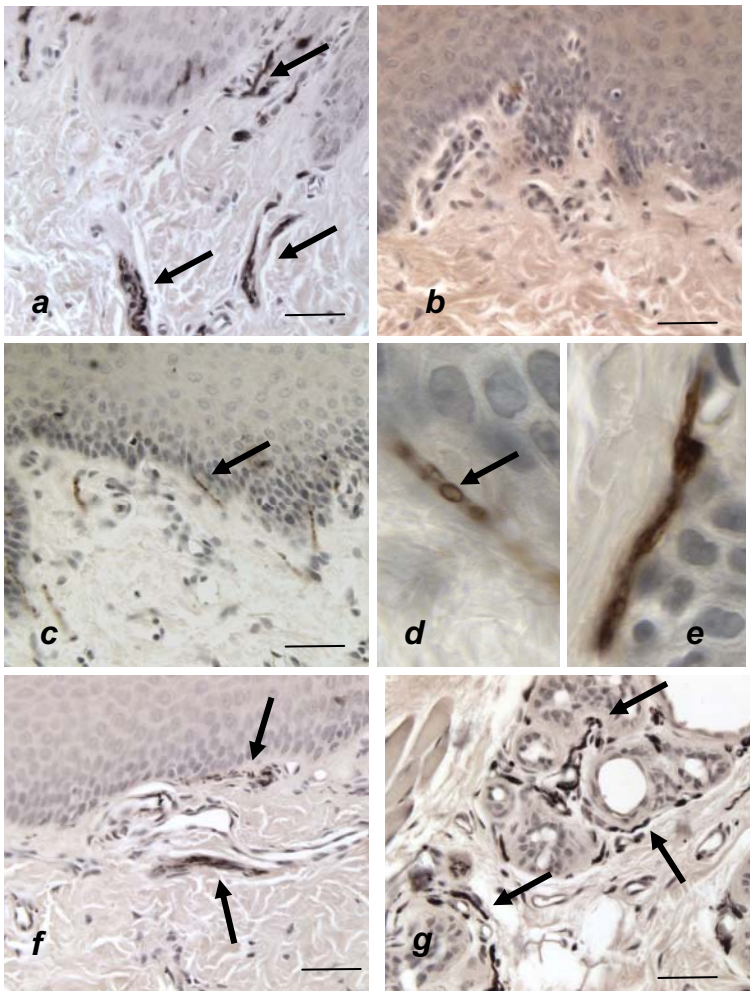

Figure 15. Reversible loss of nerve fibers following treatment with RTX. Nerve fibers are seen at the dermo-epidermal junction and in the dermis (arrows) in control and vehicle-treated hindpaws (***a***). One day after the RTX injection (1.0 μg) there are no recognizable nerve endings in the dermis (***b***, 40x). At a 10-fold lower concentration of RTX, nerve ending destruction occurs (***c***, 40x) with vesiculation of the nerve (***d***, 100x), when compared with vehicle-treated tissue (***e***, 100x). By 30 days following injection, regenerating nerve bundles with several nerve endings were present at the level of the rete ridges (***f***, 40x). Subcutaneous sweat glands are surrounded by normal nerve fibers at this time point (***g***, 40x). Bars represent 50 μm.

The transient nature of the treatment can be used in painful peripheral conditions, such as Morton's and other traumatic neuromas, diabetic neuropathy or after surgical procedures to alleviate postoperative pain [19].

3.6. In vivo experimental data: central application of RTX (intraganglionic, intrathecal)

Peripheral application of RTX showed great efficacy and reversibility. This latter phenomenon was attributed to the regenerative ability of the peripheral nerve fibers and to the

fact that peripheral injection of RTX did not induce degeneration of sensory ganglion neurons.

Calcium imaging data on DRG neuron cultures, however showed abrupt and selective deletion of vanilloid sensitive neuronal perikarya. Experiments below simulate conditions in the in vitro chambers with the goal of selective elimination of TRPV1 positive neurons.

Single intraganglionic and multiganglionic approaches were designed to test, whether the treatment can be applied in an anatomically determined way. The single intraganglionic application modeled conditions with localized painful diseases (trigeminal neuralgia, herpes zoster). The multiganglionic approach was designed to alleviate pain affecting multiple body sites keeping in mind patients, who suffer from advanced widely metastatic cancer. The multiganglionic application uses the cerebrospinal fluid (CSF), involves the use of larger amount of drug and with this increases the susceptibility for drug toxicity. Apart from efficacy, the safetiness of the application was an equally important issue.

3.6.1. Single intraganglionic injection in rat experimental model

Unilateral intraganglionic microinjection of RTX into the TG (Fig. 16, *a*-*c*) attenuated or eliminated both the afferent (nociceptive) and efferent (neurogenic inflammation) functions

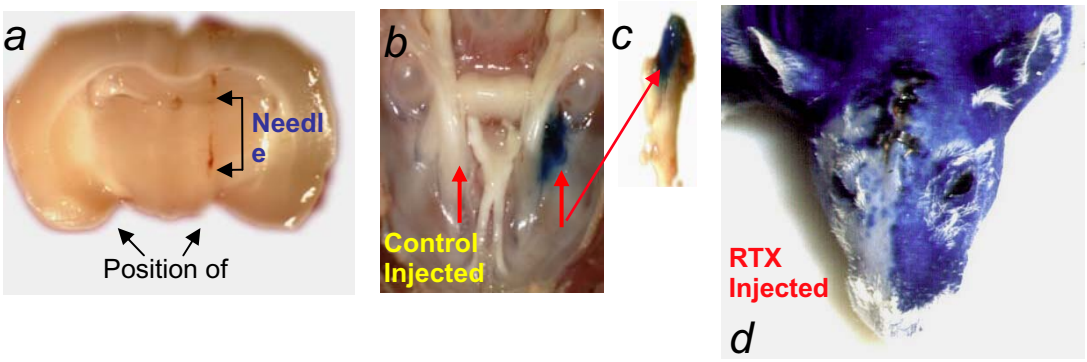

Figure 16. Single intraganglionic treatment. RTX was microinjected unilaterally into the TG using a transcranial stereotaxic approach. Coronal section of the brain at the level of the injection reveals a needle tract (***a***). Coomassie blue dye depicts trigeminal injection site at the base of the skull and TG after anatomical preparation (***b***-***c***). RTX-induced blockade of neurogenic inflammation was evaluated by extravasation of Evans blue–stained plasma proteins. Blue areas of skin identify regions with intact C-fiber innervation. Extravasation was blocked on the RTX-injected side, which remains white (***d***).

supported by C-fiber neurons (Fig. 16*d*). Intraganglionic RTX attenuated plasma extravasation; this is an indicator of neurogenic inflammation, an efferent function mediated by C fibers [32, 33]. Intravenous Evans Blue dye, which binds to plasma proteins, delineated the areas with intact innervation (Fig. 16 *d*), staining them deep blue. The skin remained largely white on the RTX microinjected side, where trigeminal neurons expressing TRPV1

were deleted. Analgesic actions were observable as soon as 24 hours after injection using a sensitive test for C-fiber function, the eye-wipe response to corneal application of capsaicin (CAP). An intraganglionic dose of 20 ng of RTX nearly eliminated the wiping behavior, and complete suppression was obtained with 200 ng (Fig. 17*a*). The antinociceptive effects from a single RTX injection were maintained for at least 1 year (Fig. 17*b*). The long duration behavioral effect and loss of TRPV1-immunoreactive (TRPV1-IR) neurons (data not shown) suggest that RTX analgesia is the result of permanent cell removal and not the result of prolonged receptor desensitization;

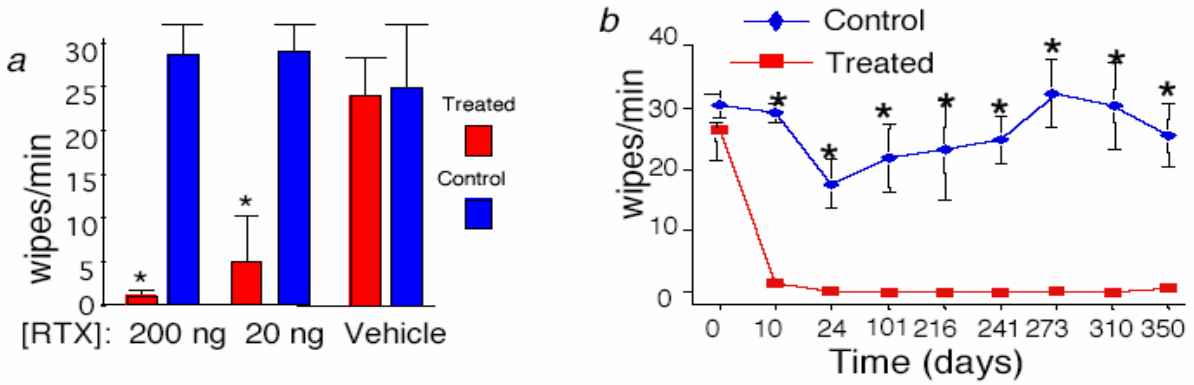

Figure 17. Dose-related blockade of nociceptive afferent transmission from the cornea after unilateral intraganglionic RTX administration. (***a***) CAP eye-wipe response was assessed 1–3 days after injection. *Pairwise *t* test; $P < 0.01$; $n = 30$, 6, and 18 for administration of 200 ng, 20 ng, and vehicle, respectively. (***b***) Block of CAP-induced eye-wipe response is evident as up to about 1 year in unilaterally intraganglionically treated rats, consistent with the permanent deletion of TRPV1-IR neurons (*repeated pairwise *t* test; $P < 0.01$; $n = 7$).

the latter phenomenon is observed when CAP is applied to neurons in acute in vitro electrophysiological experiments [34-36]. The loss of CAP chemosensitivity did not affect the mechanosensitive aspects of the corneal reflex to the liquid droplet itself. Furthermore, there were no observable alterations in grooming that might indicate the presence of a sensory dysesthesia. Intraganglionic RTX administration produced extensive deletion of TRPV1-expressing neurons and could be seen by immunohistochemistry as early as 1–3 days after RTX treatment (Fig. 18, *a–d*). To establish that another class of sensory ganglion neurons remains intact, we stained for a neurofilament protein (N52) expressed in neurons with large-diameter myelinated axons [37]. Both single- and double- stained (N52 and TRPV1) sections were examined. Injected TGs contain many N52+ neurons (684 ± 32, brown in Figure 18, *c* and *d*) but very few TRPV1+ neurons (123 ± 36, purple), while contralateral TGs show both N52+ (709 ± 23) and TRPV1+ (604 ± 68) neurons (Fig. 18, *e* and *f*). The loss of TRPV1+ neurons was significant ($P < 0.01$). The loss was also evident using RT-PCR; however, a small amount of RNA TRPV1 was detectable in the RTX-injected ganglia (Fig. 18*g*), consistent with cell counts showing

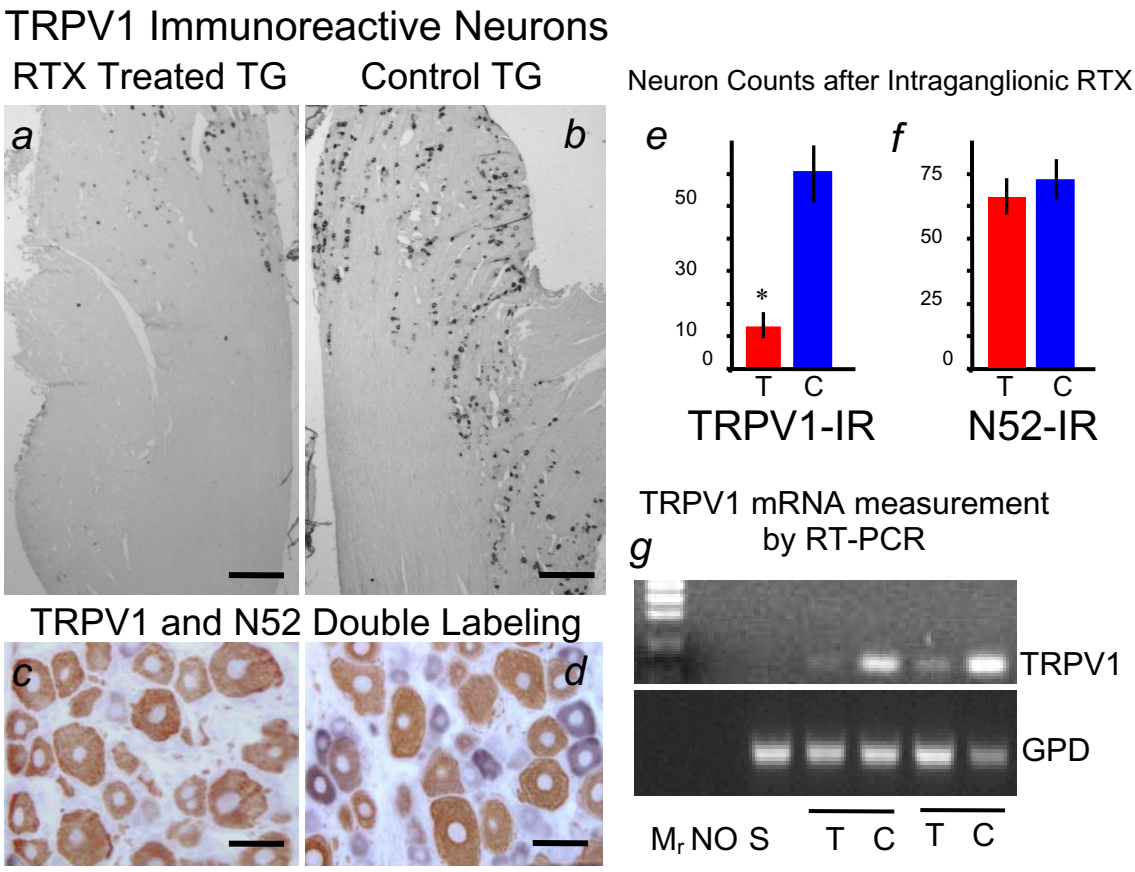

Figure 18. Selective loss of TRPV1-IR sensory ganglion neurons after RTX (200 ng) microinjection. (***a***) Immunostaining for TRPV1 shows extensive loss of IR neuronal perikarya after RTX injection compared with contralateral noninjected TG (***b***). (***c***–***f***) Double labeling shows that large myelinated N52+ sensory neurons (brown) are retained on the RTX-injected side, whereas TRPV1+ neurons (purple) are deleted (***c***). On the contralateral, noninjected side, both N52 and TRPV1 neurons are intact (***d***). Quantification shows no significant difference in the number of N52-IR perikarya after RTX, whereas an 80% reduction in TRPV1+ neurons occurs (***e*** and ***f***). Bars in graph represent the average neuron counts in three sections of TG from three to five different rats assessed between 1 and 3 days after injection (*$P < 0.01$). (***g***) RT-PCR shows reduction of mRNATRPV1 in two different rats. Mr, markers; NO, no primer; SC, spinal cord; T, RTX treated; C, contralateral TG. Bars: 0.5 mm (*a* and *b*) and 50 μm (*c* and *d*).

substantial loss of TRPV1-IR neurons and retention of the N52 neurons not expressing TRPV1 (Fig. 18, *c* and *d*).

3.6.2. Multiganglionic (intrathecal) administration of RTX in rats.

Severe pain secondary to advanced metastatic disease is generally more diffuse and not localized to one or two dermatomes. In these cases, multiple ganglia can be treated bilaterally via the cerebrospinal fluid. To test this, RTX was administered by lumbar puncture to target ganglia that innervate the tail and lower limbs. Treatment effectiveness and specificity were assessed by measuring (a) selective attenuation of noxious thermal and inflammatory responses, (b) the degree of spread of the drug by behavioral comparison to the

forelimbs, corresponding to the spatial extent of the cell deletion, and (c) retention of locomotor activity and mechanosensation. RTX administered intrathecally (10, 50 ng) produced minor increases in withdrawal latency to a radiant noxious thermal stimulus [26, 27], whereas at doses of 100 and 200 ng, many animals reached the 14-second cutoff for hindpaw and tail stimulation without affecting forepaw latencies (Fig. 19*a*). Intrathecal RTX also blocked carrageenan-induced thermal hyperalgesia, consistent with a substantial role of TRPV1 positive neurons

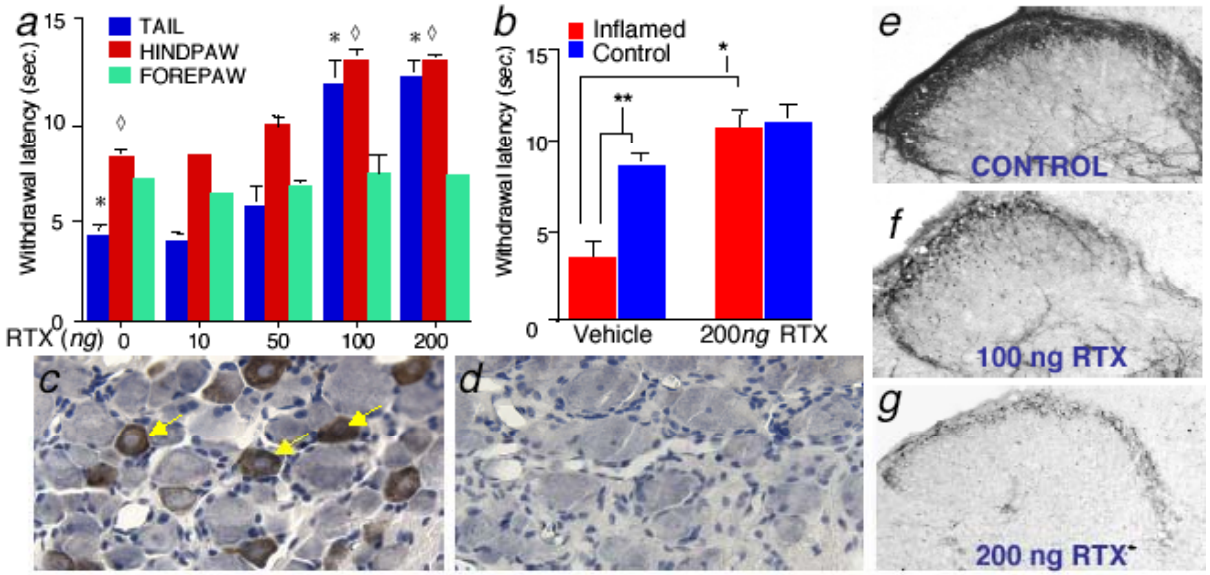

Figure 19. Intrathecal (multiganglionic) RTX attenuates thermal nociception and inflammatory hyperalgesia. (***a***) Dose–response to lumbar intrathecal administration of RTX (n = 50, 10 per group; $*^{,\#}P < 0.05$). Doses lower than 50 ng were without effect. Robust analgesia was obtained for the tail and hindpaws at doses of 100 and 200 ng. (***b***) Carrageenan inflammatory hyperalgesia (n = 4 per group; $**$ $P < 0.05$) is reversed after 200 ng intrathecal RTX ($*P < 0.05$). No analgesic effect was seen in forepaws (*a*), correlating with retention of TRPV1-IR neurons in the cervical ganglia (***c***) and their loss in lumbosacral ganglia (***d***). Dose-related reduction of CGRP-IR, a neuropeptide expressed by nociceptive afferent terminals, in the lumbar spinal cord at 3 days after administration of RTX (***e-g***).

in experimental inflammatory conditions (Fig. 19b), as shown by targeted disruption of the TRPV1 gene [38, 39]. Behavioral effects were reflected at the cellular level by decreases in TRPV1 and calcitonin gene-related peptide (CGRP) immunoreactivities in the lumbar ganglia and dorsal horn, respectively, consistent with deletion of TRPV1-expressing neurons (Fig. 19, *d-g*). In contrast, TRPV1+ neurons in cervical ganglia, which are remote from the level of lumbar RTX application, were unaffected (Fig. 19*c*), corresponding to retention of normal forepaw-withdrawal latencies (Fig. 19*a*).

Thus, by targeting one or many ganglia, using the intraganglionic or intrathecal routes, respectively, the spatial extent of the therapeutic action may be adjusted to match varied clinical presentations.

3.6.3. Retention of other somatosensory functions and locomotion.

Importantly, the response to mechanical stimuli remained intact. Orientation to and withdrawal from a pinch with toothed forceps on the tail, forepaws, and hindpaws were present in all RTX-treated animals, and responses were qualitatively similar to controls. Quantitative assessment of mechanosensation using von Frey hairs also showed no alteration in RTX-treated (3 and 10 days and 1 year) animals in comparison to control animals. No significant difference was observed in the threshold for light touch or forepaw withdrawal between untreated controls (10.9 ± 1.8 g for light touch, 20.3 ± 5.7 g for paw withdrawal), treated animals after 3 days (11 ± 1.8 g, 46 ± 30.6 g), treated animals after 10 days (10.1 ± 1.1 g, 22 ± 4.6 g) and treated animals after 1 year (11.7 ± 0.0 g, 33.7 ± 16 g). There were no indications of mechanoallodynia such as prolonged withdrawal to touch with the von Frey hairs, or mechano-hyperalgesia as assessed by withdrawal from a pinprick (all animals had a withdrawal duration of 0.5 second or less) [28]. No alteration occurred in locomotor function

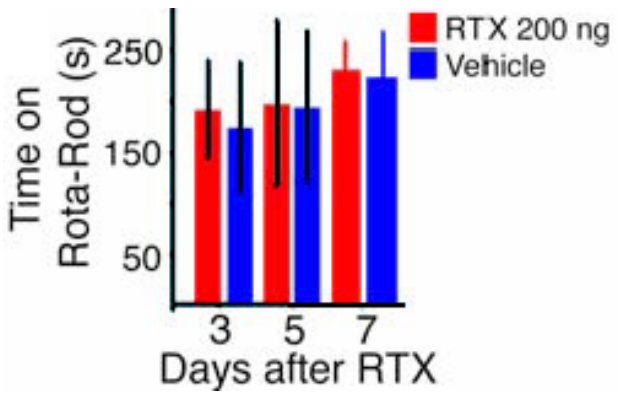

Figure 20. Testing of locomotor function on the accelerating Rota-Rod.
Locomotor function was tested in intrathecally treated animals (vehicle and 200 ng RTX) 3, 5, and 7 days after the administration of the drug. There is no significant difference between the RTX and vehicle treated animals. These results correlate with the histological and immunohistochemical findings on L4-5 dorsal root ganglia (Fig. 19, *c* and *d*), ie. the retention of large diameter neurons after RTX treatment.

as evaluated with an accelerating Rota-Rod, indicating the presence of intact motor axons and sensory proprioceptive neurons in ganglia exposed to RTX (Figs. 19*d* and 20). Normal locomotion was also evident in the canine subjects (see later). As with the trigeminal microinjections, no indications of sensory neglect or denervation induced hyperesthesia syndromes (e.g., autotomy behavior) were observed [40, 41]. These features reinforce the clinical applicability of RTX, since the pathological, inflammation-associated aspects of pain are eliminated, while mechanonociception, motor function, and other sensory modalities remain intact.

3.6.4. Veterinary clinical application.

The canine model was established to assess the efficacy of primary afferent neuronal deletion in a higher order mammal with clinical problems more closely approximating the human situation. Based on attenuation of thermal response determined in an initial cohort, a

single intrathecal dose of RTX (1 µg/kg) was administered under general anesthesia via cisternal puncture in dogs suffering from malignant neoplasms and/or osteoarthritis. Visual analog scale (VAS) ratings of nociceptive status before the injection averaged 62 ± 7.6 (mean ± SEM); these ratings sharply decreased (11 ± 3.0) at the 2-week follow-up and were maintained at 6 and 10 weeks (9.6 ± 5.3 and 7.5 ± 4.2, respectively) (Fig. 21). The animals initially presented with continuation of limb guarding (affected limb) as they walked, but this improved over time and daily activity increased, as was evident from video recordings. In fact, the entire demeanor of the dogs appeared improved following intrathecal RTX treatment. The efficacy of RTX action was further demonstrated by (a) the discontinuation or greatly reduced use of supplementary analgesics (opioids and NSAIDs in all eight dogs) and (b) the fact that neoplastic advancement did not diminish the RTX-induced analgesia.

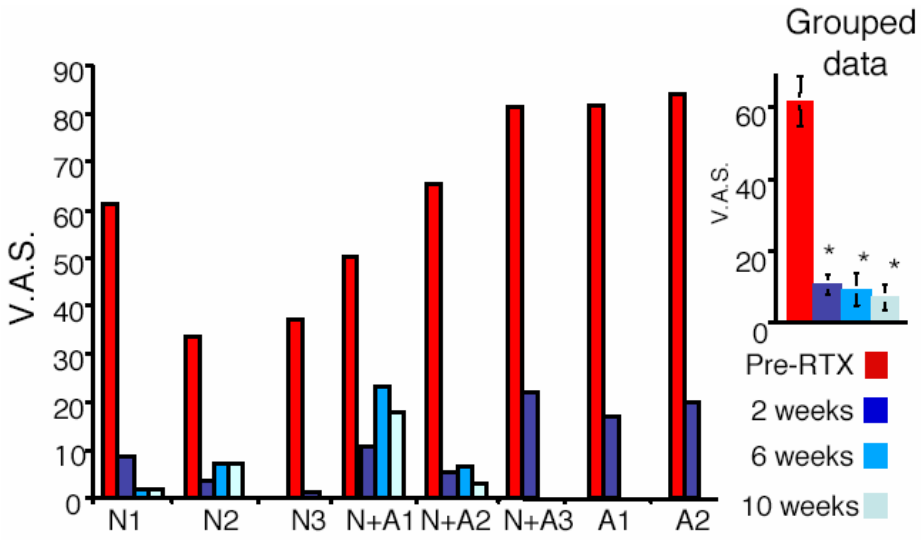

Figure 21. RTX analgesia in naturally occurring neoplasms or osteoarthritis in the dog. Intrathecal RTX reduced pain reports by the owners using a VAS in neoplastic (N), arthritic (A), and neoplastic plus arthritic (N + A) dogs (n = 8). Bars represent individual animals; inset represents summed data (*ANOVA with Scheffe's post hoc test; $P < 0.05$).

3.6.5. Comparative histology of rat and canine sensory ganglia after RTX treatment

Comparative histology of rat and canine sensory ganglia demonstrated that RTX eliminated many small-diameter neuronal cell bodies in both species, leaving no visible damage to surrounding neuropil (Fig. 22, *a–h*). The early morphological signs of specific cell deletion were studied in rats sacrificed at 6, 12, and 24 hours. During this period, nuclear envelope ruffling and displacement of the nucleus in specific ganglion neurons were noted, indicating early stages of neuronal damage (Fig. 22, *a* and *b*). In dogs, satellite cell activation and neuronophagia occurred around the dying neurons 3 weeks after intrathecal RTX treatment,

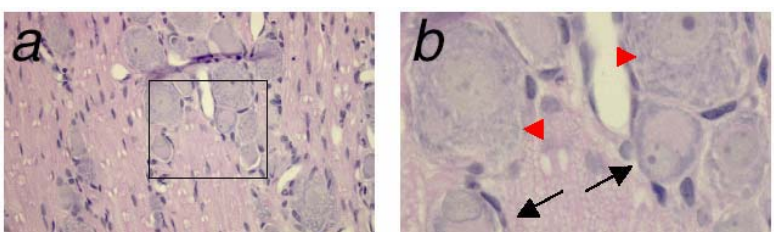

Figure 22. Morphological aspects of cell deletion in rat TG and dog DRG over time.
(***a***) High-power (x40) image of an adult rat TG, 24 hours after 200 ng intraganglionic RTX administration, shows grossly normal appearance. (***b***) Higher power, however reveals swollen eosinophilic cytoplasm and dislocated nuclei with partial wavy pattern of the nuclear membrane in many small- to medium-sized neurons (black arrows), characteristic of calcium cytotoxicity. Large neurons (red arrowheads) are normal. (***c***) DRG from an adult dog 21 days after intrathecal RTX injection shows patchy proliferation of satellite cells. (***d***) At higher magnification, neuronophagia is evident (black arrows). A necrotic neuron in which the nuclear membrane is faintly visible around a spot of condensed nuclear material is also visible (red arrowhead). By 30 days in dog ganglia, damaged and dead neurons are replaced by proliferating satellite cell colonies called nodules of Nageotte, which can be seen as a ball of proliferating cells (***e*** and ***f***). (***g***) One year after RTX treatment, the rat TG shows extended areas of acellular eosinophilic fields surrounded by rosetting satellite cells, indicated by red asterisks at higher magnification (***h***). There is no evidence of excessive, distorting glial proliferation. Bars: 100 μm (***a***, ***c***, ***e***, and ***g***); 25 μm (***b***, ***d***, ***f***, and ***h***).

progressing into characteristic nodules of Nageotte, which have been described in human diseases with pathological sensory aspects (Fig. 22, *c-f*) [42]. After 1 year, retention of the large-size neurons and deposition of fine extracellular matrix inside satellite cell rosettes were observed in rat ganglia without abnormal scar formation (Fig. 22, *g* and *h*).

3.7. Effect of RTX on human DRG neurons.

The ligand-activated cell deletion approach for pain control is based on the enriched expression of TRPV1 in a subset of sensory ganglion neurons. Immunocytochemistry and live-cell imaging were performed to determine expression of TRPV1 in adult human sensory ganglia and demonstrate whether selectivity can be expected upon administration into humans

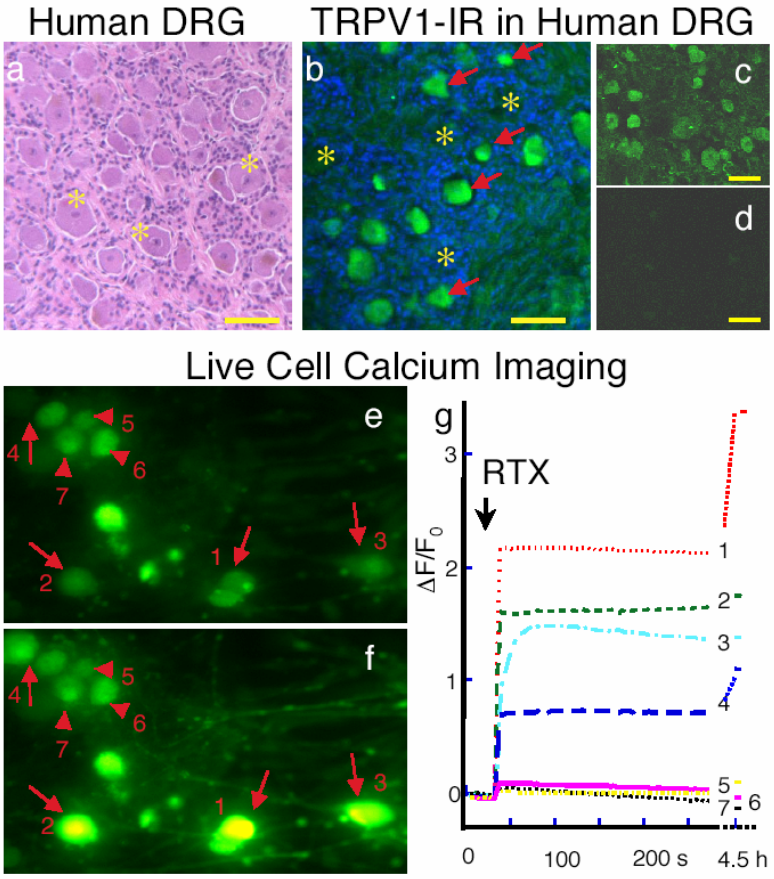

Figure 23. Human DRG neurons show selective sensitivity to RTX treatment.
(***a***) H&E section, adult human DRG (* large sized neurons). (***b***) Green immunofluorescence human TRPV1-IR neurons (arrows), contrasted with satellite cell nuclei (blue). (***c***) TRPV1-IR (green) is adsorbed by the peptide antigen (***d***). Selective response of human embryonic DRG neurons to RTX assessed by increases in $[Ca^{2+}]_i$ using Fluo-4 AM imaging (***e*** and ***f***). Arrows indicate responding neurons, and arrowheads indicate nonresponding neurons. ***e*** shows the baseline fluorescence depicted as near 0 for the first 30 seconds of the normalized data in the graph (***g***). In *f*, the transmembrane calcium flux leads to increases in intracellular calcium in specific neurons, which become brightly fluorescent (20x objective). (*g*) Traces of individual cells showing a substantial and abrupt response in vanilloid-sensitive sensory neurons (traces 1–4). Elevation of $[Ca^{2+}]_i$ for a prolonged period of time is suggestive of imminent cell death in cells responding to vanilloid treatment. The RTX effect is clearly selective; nonresponding cells (traces 5–7) maintain normal calcium levels. Increase in normalized fluorescence intensity (numbered $\delta F/F_0$ traces refer to cells in *e* and *f*). Bars: 100 µm.

(Fig. 23). While the cloned human TRPV1 has been studied in heterologous expression systems [43] and in an immortalized human neuronal cell line [44], there are no data on the physiological response and selectivity of primary human DRG neurons to stimulation by vanilloids. Figure 23, *a* depicts the microscopical structure of a normal adult human DRG and

shows variably sized neurons surrounded by satellite cells. Immunofluorescence studies for the human TRPV1 reveals two cell populations: neurons showing positive (green) labeling over their perikarya and cells with negative results. These later population is depicted as "empty" lacunae surrounded by Hoechst 33342+ satellite cells (blue) are occupied by neurons, which are negative for human TRPV1 expression.

In vivo calcium imaging on human DRG neurons shows a dramatic response to RTX (Fig. 23, *e-f*). Resiniferatoxin opens the human TRPV1 ion channel and increases the $[Ca^{2+}]_i$ inside human TRPV1+ DRG neurons. This change of $[Ca^{2+}]_i$ can be detected with Fluo-4 AM, which changes its fluorescence emission intensity according to the $[Ca^{2+}]_i$ (Fig. 23, *e–g*). Fluo-4 AM imaging clearly distinguishes two populations of neurons: vanilloid sensitive and vanilloid insensitive. The $[Ca^{2+}]_i$ in responding human neurons (Fig. 23, *e–g*; cells 1–4) remains high for a prolonged period of time, suggesting a damaged, incapacitated state and imminent cell death. The images and line traces from non-responding cells (Fig. 23, *e–g*; cells 5–7) are also important, since they demonstrate the selectivity of the RTX treatment and the lack of toxicity to the non-responding neurons or satellite cells.

4. DISCUSSION

4. 1. Molecular and in vitro experimental data for the characterization of TRPV1

4.1.1. TRPV1 recombinants for the study of vanilloid-triggered cellular events

The vanilloid receptor 1(TRPV1/VR1) is a ligand activated mixed cation channel, which belongs to the Transient Receptor Potential (TRP) channel family. The first part of the thesis investigates the cellular dynamics of vanilloid-triggered events through *in vivo* expression of fluorescent- and epitope-tagged recombinants of rat TRPV1. Extension of the C terminus with the 27-kDa eGFP did not compromise the electrophysiological function of TRPV1 upon expression in heterologous cell systems and tagging with either eGFP or a short 12-amino acid ε-epitope did not affect vanilloid-induced channel opening as assessed by $^{45}Ca^{2+}$-uptake. The ultrapotent vanilloid, RTX, binds with nanomolar affinity to both TRPV1eGFP and TRPV1εMTH. The binding and $^{45}Ca^{2+}$ uptake parameters are similar to those reported either for the non-chimeric TRPV1 or for rat DRG primary cultures [45-51]. The electrophysiology of TRPV1eGFP-expressing cells showed that vanilloids rapidly induced an inward current flow that was blocked by CPZ, as described for wild-type TRPV1 [16]. Vanilloid induced $^{45}Ca^{2+}$ uptake and [^{3}H]RTX binding were also inhibited by CPZ, further supporting the specific interaction of vanilloids with the tagged TRPV1 variants. TRPV1eGFP and TRPV1εMTH mimic the wild-type receptor and are thus useful reporters

with which to study the dynamics of TRPV1 activation by vanilloids, other modulators, and physical stimuli.

4.1.2. Cellular localization of TRPV1

High-resolution confocal fluorescent microscopy was employed to study the cellular distribution of TRPV1. In addition to localization at the plasma membrane, TRPV1eGFP was evident on ER structures. The ER localization was confirmed by using eGFP tagged with the ER retention signal (KDEL motif) and even more specifically with the ER Tracker Blue-White, a vital ER-labeling fluorescent dye (Fig. 4, *h* and *i*). Likewise, the ER lattice was also readily apparent when TRPV1eGFP was transiently transfected into DRG neurons, although the size and spherical geometry in sensory neurons makes it difficult to achieve resolution similar to the COS7 cells (data not shown) [31]. These results are consistent with the dense neuronal intracellular staining seen in sections of trigeminal ganglia after fixation and immunostaining of tissue sections for TRPV1[15, 52]. The ER localization was evident using different cell lines in the study including COS7, HEK293, and NIH 3T3 cells.

4.1.3. Early cellular events associated with TRPV1 activation

Fluorescent Ca^{2+}-imaging and $^{45}Ca^{2+}$-uptake experiments confirmed that vanilloids (CAP, RTX, olvanil or anandamide) induce large increase of $[Ca^{2+}]_i$ in TRPV1 expressing cells[18]. Fluorescent labeling of TRPV1 demonstrated abrupt ER fragmentation due to agonist treatment. The increase of $[Ca^{2+}]_i$ upon addition of vanilloid agonists to TRPV1-expressing cells coincided with the rapid transformation of the normal lattice like ER membrane structure into rounded vesicles as the earliest hallmark of Ca^{2+} cytotoxicity. Calcium-induced ER vesiculation occurred throughout the cytoplasm (*i.e.* the *z*-stack of confocal acquisition), similar to that described previously for ionomycin [30]. This type of membrane rearrangement (Figs. 4 and 5) is clearly distinct from the agonist-mediated endocytosis, which can occur with non-ion channel transmembrane receptors.

In addition to the ER, live cell imaging experiments revealed important role of the mitochondria in TRPV1 expressing cells. The intracellular location of TRPV1 was separable from the mitochondrial compartment as assessed concurrently with the red MitoTracker dye (Figs. 4 and 7). Although spatially distinct, both the ER and mitochondria changed conformation in seconds upon vanilloid activation (Figs. 4, 5, and 7).

The staining of the mitochondrial compartment with the MitoTracker vital dye provided a surrogate end point to extend our findings in transiently transfected cells to DRG neurons in primary culture where specific small sized neurons showed the same immediate early changes in mitochondrial structure when exposed to vanilloids (Figs. 4, *f* and *g versus*

7). However, the perikarya of the responding neurons are spheroid rather than flat and extended, and a much smaller volume is available for confocal microscopy due to the high nucleus/cytosol ratio. Thus, in contrast to the flattened COS7 cells, geometry and size make nociceptive neurons less favorable subjects for live cell imaging of elongated organelles such as the mitochondria and the ER. As expected for the restricted cellular expression of TRPV1 in the DRG [16], RTX did not affect the mitochondria of adjacent large neurons or glia, imaged at the same time (Fig. 7).

4.1.4. Extended confocal imaging depicts receptor specific cell death

Imaging studies on transfected cells with TRPV1-eGFP confirmed specific action of RTX on TRPV1 expressing cells. Mitochondria remained unaltered during vanilloid challenge in non-transfected bystander cells or in neurons and glia not expressing the receptor. Extended confocal imaging on TRPV1-eGFP positive cells after vanilloid treatment showed (i) shedding of the plasma membrane; (ii) conformational changes of mitochondria; and later (iii) blebbing of the nuclear envelope, (iv) rupture of the plasma membrane (Figs. 5 and 6). Accumulation of propidium iodide (PI) in the cell nucleus was also observed. The effects were entirely specific for transfected cells (transient or permanent), since the mitochondria remained intact and there was no evidence of PI positive nuclei in these cells.

To prove the same specificity and efficacy exist in neurons endogenously expressing TRPV1 ratiometric calcium imaging was combined with fluorescent imaging for PI in rat DRG cultures. Indo-1 imaging confirmed the specific activation pattern, since only a subset of neurons responded with increase of $[Ca^{2+}]_i$ to RTX treatment (Fig. 8). The $[Ca^{2+}]_i$ level remained high for an extended time and culminated in the death of the neurons depicted by PI positive nuclear staining. The selectivity is apparent since adjacent non-TRPV1-expressing cells (large diameter neurons and glia) remained resistant to PI permeation.

4.1.5. Studies on $TRPV1_{ER}$

Although, the ER localization of TRPV1 may not be surprising, due to protein synthesis in general, finding functionally active receptor at this site intrigued us. Imaging studies in calcium-free media on TRPV1-eGFP transfected Cos7 cells showed vanilloid-induced remodeling of the ER. The changes were similarly to that observed in normal calcium conditions [18], however the rate was markedly slower (data not shown). Ca^{2+}-imaging studies in "zero" ($<10^{-7}$ M) extracellular calcium levels together with blockade of the plasma membrane localized receptor ($TRPV1_{PM}$) by ruthenium red (RR) revealed calcium fluxes originating from intracellular stores in vanilloid sensitive DRG neurons upon administration of RTX. This vanilloid-regulated pool almost entirely overlaps with the thapsigargin (TG)

sensitive intracellular calcium store, which functionally defines the ER pool. This store can be reversibly depleted and replenished with CAP, however, RTX applied at high concentration (~1.6 μM) leads to irreversible depletion of this store (Fig. 9) [26]. Therefore, the mechanism of the RTX-induced cell deletion in vanilloid sensitive cells can be at least partly attributed to incapacitation of the calcium regulation mechanisms of the ER. The ER-localized TRPV1 pool ($TRPV1_{ER}$) was evident along the neuronal axonal and dendritic arborizations. Signaling through $TRPV1_{PM}$, and $TRPV1_{ER}$ can regulate meticulously the Ca^{2+}-homeostasis within the nociceptive neurons including the peripheral endings. This fine regulation is of paramount importance since over-activation as in a chronic pain state, can lead to calcium overload, and result in peripheral nerve terminal inactivation. These experiments also highlight the critical role of the ER during vanilloid agonist treatment and provide further evidence to Berridge's "neuron-in-neuron" concept, which confers the ER with different and crucial signaling functions in addition to its role in protein synthesis [53].

These data argue against specific TRPV1 proteolysis or desensitization of TRPV1 by limited endo- or exocytosis as mechanisms mediating TRPV1 protein elimination from the primary cultures. Several mechanisms can govern the intracellular remodeling and cell death that occur upon exposure to vanilloids. The most likely is rapid Ca^{2+} toxicity following TRPV1 activation, which is consistent with the data presented here from TRPV1-expressing cells and DRG neurons (Figs. 4–8) and by others [16, 54]. Although the primary steps of Ca^{2+} toxicity are similar to apoptosis, including nuclear blebbing and PI staining of the nucleus [55], chromatin fragmentation, apoptotic body formation, and caspase activation were not apparent within 24 h (data not shown). Previous studies characterized only the terminal phase of vanilloid-induced cellular changes in detail. The longer term dynamics visualized with TRPV1eGFP in the present study are consistent with those noted with end point observations in the DRG, including intracellular membrane fragmentation, mitochondrial swelling, and nuclear envelope segmentation [55-58]. By extension, these results are generalized to a variety of ligand-operated Ca^{2+} channels such as the excitatory amino acid *N*-methyl-D-aspartic acid receptor, which can be activated by potent toxic ligands [59, 60].

4.2. In vivo studies for the characterization of RTX action

4.2.1. Peripheral application of RTX

Topical capsaicin therapy has been proposed for persistent painful disorders [61], however, the relatively weak potency, the need for multiple applications and the algesic effect limits its use as a first line analgesic. In contrast, a single application of RTX can produce long-lasting analgesia when administered epidurally (>60 μg,) or by a subcutaneous systemic

route (10–300 μg) [22].

This study demonstrates that a single, peripheral injection of RTX (0.0625-10 μg) can produce a reversible, localized analgesic effect through reversible destruction of the nerve terminal endings. RTX induces a large intracellular increase of calcium via the TRPV1 receptor that renders the nerve ending non-responsive [18, 31, 52, 62, 63]. While the distantly located perikarya are preserved from calcium cytotoxicity, loss of peripheral C-fiber endings prevents action potential generation. Temporary removal of nerve endings of C-type and probably a small population of A-δ nerve fibers provides a mechanism for analgesia as demonstrated in this study using a single dose of RTX and in other studies with repeated capsaicin treatments [64]. Specific anatomic targeting of TRPV1 containing C-fibers in this context provides a number of therapeutic advantages for the utilization of RTX in the treatment of pain including: (1) single dosing producing long duration pain inhibition; (2) a peripheral site of action and minimization of central nervous system involvement; (3) preservation of other sensory modalities due to inactivation of only TRPV1 expressing nerve terminals; and (4) selective inhibition of inflammation-induced pain. The specificity of RTX binding to TRPV1 expressing neurons provides a highly selective agent for analgesia. This fiber specificity allows for the maintenance of motor neuron activity and indeed, we did not observe motor deficits in any of the animals after peripheral application of RTX. Tactile sensations and mechanical sensitivity (i.e. response to high threshold pinch and von Frey stimulation) were not affected following RTX injection, supporting the idea that these sensations are not mediated by TRPV1 expressing neurons [65]. Although RTX has been reported to be a neurogenic inflammatory agent [17], we noted no edematous changes at the site of injection. RTX was able to block the development of heat hyperalgesia associated with carrageenan-induced inflammation, even though the remaining sequel (edema, erythema) of the inflammatory pathway remained intact. This blockade is remarkable given the strong hyperalgesic response normally seen following carrageenan-induced inflammation.

4.2.2. Central application of RTX: single intraganglionic injection

Peripheral application of RTX resulted in a profound, but reversible block of pain sensation (heat, inflammation). The in vitro results on heterologous cell systems and on DRG neurons (Figs. 4 and 8) suggested that application of RTX close to the cell body would lead to specific elimination of small diameter neurons together with irreversible action on pain sensation. In several clinical settings (trigeminal neuralgia, herpes zoster, Pancoast tumor, and metastatic malignant disease), this type of pain block would be sought after, since other important functions such as epicritic sensations, sensation for mechanical and high

temperature heat pain and the motor function would remain intact. The aim was to anatomically target the action of RTX and test, whether the injection has any side effect especially on the central nervous system. The specific location and specialized function of the trigeminal ganglion allowed us to test the above criteria. It was relatively easy to access and test sensory functions via the afferent fibers of the cornea and conjunctiva repeatedly during an extended period. Trigeminal injection of RTX resulted in elimination or substantial reduction (depending on the dose administered) of chemical pain sensation as well as blockade of neurogenic inflammation. The anatomical targeting was precise, only the ipsilateral side was affected. RTX elicited a substantial reduction or total elimination in chemical nociception as tested with the capsaicin eye-wipe test. Remarkably, all the injected animals responded with a few blinks after the capsaicin solution was squirted to the eye arguing for intact touch sensation. The blinking behavior, however, was not associated with wiping or squinting of the animals. The intraganglionic injection remained localized as the contralateral side reacted as normal control animals or animals treated with the vehicle only. Neurogenic inflammation, tested by extravasation of Evans blue after the application of capsaicin cream to the skin clearly delineated the borders of the treatment. The RTX injected side remained white due to lack of efferent nerve function, whereas the control side neurogenic inflammation led to leakage of the plasma proteins from capillaries together with Evans blue. There was no associated autotomy behavior, neuropathic pain, problems associated with grooming or grow of hair or whiskers. Animals were repeatedly tested as long as one and a half year (non-published data) with no change in their behavior. This profound effect was due to selective destruction of small diameter neurons in the trigeminal ganglia. Animals sacrificed as early as 24 h after RTX injection showed significant reduction of TRPV1 immunoreactivity in the trigeminal ganglia (Fig. 18). The mRNA level of TRPV1 closely followed these changes, detected by RT-PCR experiments. Consistent with the behavioral data (intact epicritic sensation, high threshold pain sensation) and confirmed by the N52 immunostaining, the large diameter neurons remained intact. The intratrigeminal RTX treatment is irreversible as evidenced by the long duration behavioral data (one and a half year) as well as the histochemical and immunohistochemical studies showing significant decrease of TRPV1 immunoreactive neuronal perikarya at the affected side [52]. Similar data was collected from non-human primates injected with RTX into the trigeminal ganglion. The effect was long lasting and there were no signs of pathophysiological (e.g.: loss of lacrimation, keratomalacia) or behavioral (e.g.: autotomy) abnormalities [66]. These findings are in agreement with our initial goals to establish an effective, long lasting, anatomically targetable treatment with minimal or no side effects.

4.2.3. Central application of RTX: multiganglionic application of RTX

Localized pain problems can be approached via peripheral or intraganglionic administration of RTX. Severe pain affecting multiple body sites, such as metastatic cancer pain or severe polyarthralgias requires a slightly different approach. Metastatic cancer can elicit pain by disturbing the vascular and lymphatic circulation around nerve bundles, compressing fibers leading to demyelination or by direct nerve fiber destruction. Infiltrating tumor cells or cells activated by tumor progression can also secrete active cytokines that irritate or sensitize the nearby nerve endings [67-70]. TRPV1 has paramount role in the sensation of inflammation-associated pain. Experiments on the TRPV1 knockout mouse or the studies presented above [38, 63] argue for the effectiveness of RTX in these conditions.

Multiganglionic administration was performed by intrathecal infusion of RTX. The concentration dependence, the effectiveness of the therapy for heat and inflammatory hyperalgesia, the spatial extent of the treatment and the retention of other sensory functions including locomotion were tested. Intrathecal RTX remained localized to the lumbar region with the specified concentrations and volume used, as there were significant differences between the front and hind paws measured with the radiant heat test. Accordingly, TRPV1+ neurons were specifically eliminated from lumbar dorsal root ganglia (Fig. 19*d*).

Similarly, to the results obtained with the peripheral application, RTX was extremely effective in blocking the inflammatory pain elicited by carrageenan. Control animals had marked guarding behavior of the injected limb with severe limping and pronounced hyperalgesia with the radiation heat test. To the contrary, RTX treated animals did not guard the limb, did not limp and showed normal or even slightly increased paw withdrawal time in the radiation heat test. Remarkably, RTX only tackled the aspect of pain of the carrageenan-induced inflammation, the swelling, redness and the increased temperature of the limb were similar in RTX treated and in control animals.

Somatosensory functions including response to touch or pinprick were also maintained after RTX treatment. The orientation towards the stimulus remained intact and there was no evidence of mechanical allodynia or mechanical hyperalgesia tested several time points. The RTX injected animals also maintained normal locomotion tested on the accelerating Rota-Rod, which signifies that the proprioceptive neuronal circuits were intact. This later was also confirmed by immunohistochemistry, which showed preservation of large diameter neurons responsible for epicritic sensations, including proprioception at the lumbar levels (Fig. 19*d*, and 18, *c* and *d*).

The multiganglionic treatment was also tested in canine patients suffering from naturally occurring conditions, such as osteoarthritis and cancer related pain. In both of these

conditions, the treatment proved to be highly effective in reducing pain sensation. This is a remarkable fact, since the majority of the new candidate analgesics poorly perform in clinical trials. It was also remarkable that the progression of malignant disease did not necessitate the administration of additional RTX or analgesics. Histology on DRGs taken from canine patients treated with RTX revealed specific neuronal damage and loss with changes of repair.

4.3. Human in vitro experiments

The ultimate objective of this study was to design new therapeutic modalities for the treatment of severe intractable pain presenting in humans. Neuronal cell deletion may seem too extreme as untoward side effects due to loss of function are feared, however the specific expression pattern of TRPV1 in a subset of DRG neurons made this approach a promising one[16]. The encouraging in vitro cellular results in TRPV1 expressing cells prompted us to test the efficacy and safety of RTX in vivo animal models[18, 52, 62, 63]. The imaging findings together with the histopathological and immunohistochemical assessment of treated animals were nicely paralleled by the in vivo data in rats and in the clinical canine subjects. Additional translational results on human TRPV1 expressing cells were essential to predict the in vivo the efficacy, specificity, and safety of RTX in humans.

Smart and his colleagues presented in vitro cellular data on the cloned human TRPV1 expressed in human embryonic kidney (HEK293) cells and proved that RTX is a potent and full agonist of the receptor [43]. We were able to demonstrate the presence of TRPV1 in human DRG ganglia and established a primary neuron culture from human embryonic DRG to predict efficacy and establish whether the same selectivity occur in humans upon administration of RTX [52]. Imaging results on human DRG neurons (Fig. 23) showed that only a subset of neurons responded with elevation of $[Ca^{2+}]_i$ to the administration of RTX. Figure 23 reveals immediate and sustained increase in $[Ca^{2+}]_i$ in a subset of neurons leading to calcium cytotoxicity and incapacitation of the responding cells. Non-responding neurons did not show change in $[Ca^{2+}]_i$. This later finding is of great importance since it predicts selectivity and safetiness of RTX treatment in humans.

5. CONCLUSIONS

The data presented in the thesis demonstrate the fundamental role of the vanilloid receptor 1 (TRPV1/ VR1) in the pain pathway and how molecular and cellular knowledge can be exploited for therapeutic intervention. Molecular engineering combined with high-resolution imaging data shed light on the intracellular localization of TRPV1. The receptor was found on the plasma membrane ($TRPV1_{PM}$) and also on the endoplasmic reticulum ($TRPV1_{ER}$) [18]. The former thought to be obvious; however, the later is an intriguing new

finding. The endoplasmic reticulum localized receptor is functionally active; it controls a calcium store that almost totally overlaps with the thapsigargin sensitive calcium pool. This internal store can be irreversibly depleted with the application of high concentration of RTX. $TRPV1_{ER}$ is also evident in axonal and dendritic projections of vanilloid sensitive neurons [31]. Application of vanilloids leads to membrane remodeling in cells expressing TRPV1, affecting the ER and mitochondrial membranes. These changes coincide with the elevation of intracellular calcium levels. Calcium imaging combined with high-resolution confocal imaging on cells ectopically expressing the vanilloid receptor and on DRG neurons confirmed that elevation of intracellular calcium by RTX incapacitates cells terminating in selective elimination of TRPV1 positive cells or destruction of peripheral nerve fibers [18, 62]. The specific expression pattern of the vanilloid receptor, as well as the selective action of the ultrapotent vanilloid agonist resiniferatoxin -tested on various in vitro model systems- allowed us to design in vivo studies with relevance to painful conditions occurring in animals and in humans [52, 63].

The in vivo data demonstrate the crucial and necessary role that TRPV1+ neurons play in supporting nociception arising from inflammatory hyperalgesia, osteoarthritis, and cancer, and how this can be exploited to produce a new class of pain treatments. The RTX intervention removes the “C-fiber line of communication” but is not equivalent to drugs that block one of the multiple neuroactive substances these neurons release or respond to (e.g., substance P, CGRP, glutamate, bradykinin, prostaglandins). The diversity of transmitters and receptors involved in pain generation suggests that blocking only one element may not yield effective analgesia [6, 14, 71]. In contrast, eliminating the participation of TRPV1-expressing neurons at either the nerve ending or the perikarya reveals the algesic profile of these neurons and their potential as pharmacological targets. Furthermore, the present chemical cellular knockout is not equivalent to removal of the TRPV1 molecule in TRPV1 KO mice [38, 39], although the behavioral repertoire seen with RTX-neuronal deletion is quite similar and reinforces the idea that TRPV1 is a key molecule in transduction of nociceptive stimuli.

In vivo experiments demonstrate the behavioral effectiveness of RTX, and immunohistochemistry confirms that RTX destroys peripheral nerve endings or deletes TRPV1+ neurons. Our results are consistent with earlier in vitro observations of CAP/RTX-mediated damage and elimination of cultured rat DRG neurons or cells ectopically expressing TRPV1 and do not appear to support a receptor desensitization mechanism for the analgesic actions [36, 72-75]. The potency of RTX yields a duration and degree of intracellular calcium elevation that makes it fundamentally more efficacious for cell deletion in adult animals than CAP, which while highly algesic [76], is a readily reversible agonist of TRPV1 [18, 77, 78].

The data presented here suggest that cellular excision by “molecular neurosurgery” would confer several advantages over neurosurgical, chemical (phenol, ethanol), or radiofrequency neuroablative techniques in terms of selectivity, efficacy, and lack of side effects. RTX removes one class of neurons, whereas the other treatments lack sensory modality selectivity, and, if motor axons are compromised, bring about loss of muscular control. Conventional ablative approaches often yield incomplete relief or evolve into a deafferentation pain syndrome [79]. Indiscriminate destruction of ganglionic neurons produces extensive proliferation of glia, inflammatory, and connective tissue cells, leading to scar formation and neuropathic sensory problems [79, 80]. RTX excises the TRPV1+ neurons in such a way that formation of abnormal anatomical structures is circumvented. In RTX-treated animals, the lack of chronic behavioral maladaptations also may be due to retention of afferents not expressing TRPV1, incomplete removal of C-fiber neurons, and the fact that C-fiber primary afferents ascend and descend five or more dermatomes [81]. All of these influences may prevent trophic disturbances and secondary neuronal alterations due to loss of synaptic contacts. Furthermore, TRPV1 cell deletion is not equivalent to peripheral nerve axotomy. Formerly, researchers had thought that rearrangement of A-δ fibers occurred upon damage to peripheral nerve, which stimulated collateral sprouting of A-beta fibers into the superficial dorsal horn and conferred mechanosensitive allodynia and abnormal behaviors in animals (autotomy) [40, 82]. Recent evidence by Santha and Bao suggests that sprouting is substantially less than originally reported [83, 84].

Deletion of nociceptors is especially effective in blocking inflammatory hyperalgesia in rats and clinical manifestations of pain in dogs. However, the loss of the TRPV1+ nociceptors does not eliminate all types of pain sensation. Many animals remained responsive to thermal stimuli, and not all went to the behavioral cutoff. No significant alteration in response to noxious mechanical sensation was detected, as was also noted with intrathecal administration of CAP [73], indicating the presence of a population of high-threshold mechanoreceptive afferents that do not express TRPV1. No tendency to increased sensitivity to mechanical stimuli (von Frey hairs or withdrawal duration after pinprick) developed, suggesting that TRPV1-neuronal deletion, as performed here, does not induce a neuropathic pain state [85].

The anatomically directed nature of RTX administration allows the treatment to be tailored to the site (or sites) of nociceptive generation using interventional procedures with either a reversible or irreversible outcome as the therapeutic goal. Routes of administration can include peripheral, single or multiple intraganglionic injections or intrathecal application for disseminated pain problems. In all cases, the same principle of receptor-mediated Ca^{2+}

cytotoxicity is operative [85], but the present data show that the distal (peripheral) injections do not eliminate the TRPV1-expressing DRG neurons, and therefore the analgesic effect is transient[52, 63]. The peripheral data support a spatially delimited Wallerian-like degeneration occurring locally and specifically in vanilloid-sensitive fibers [63, 86]. Because the damaged ending remains connected to an intact cell body, the ending reinnervates the skin, a process that requires approximately 20 days in the present study. This reinnervation is consistent with studies of topically applied CAP [64] and recent data using RTX [63]. Myelinated fibers are not affected as was reported earlier with CAP [87]. The extent of the reversible degeneration correlates with the RTX application. Peripheral administration of comparatively low doses of RTX demonstrates that regional specificity can be achieved, thus highlighting an important advantage of this strategy over systemically acting analgesic agents (e.g. opioids). Local administration yielded lateralized effects that were confined to the injected hindpaw and ipsilateral spinal cord. The nerve terminal inactivation was specific to heat-sensing and inflammation-responsive nociceptive afferents, while neither the response to mechanical touch nor performance of a demanding motor task was affected. Peripheral RTX also blocked stimulus-transcription coupling of immediate early gene expression (c-Fos immunoreactivity) in spinal cord second order neurons after inflammation. The peripheral data demonstrates the power of reversible inactivation of the small diameter fiber component using RTX and may provide a potential approach for intermediate duration pain control such as trauma, neuropathic and postoperative pain[19].

While the intraganglionic and peripheral injections are well localized, the intrathecal and intracisternal routes have the potential to reach the brain via the cerebrospinal fluid. We observed no behavioral abnormalities in RTX-treated rats. In the dogs, even with intracisternal administration, there were no reports of abnormal personality changes. RNA blot [16] and our own immunohistochemical studies have not detected TRPV1 expression in brain regions or immunopositive neurons (data not shown). The lack of behavioral alterations suggests that, despite reports of CAP actions [88, 89], RTX-binding sites [90], or TRPV1 expression [91], higher brain centers are not substantially affected upon intracisternal or intrathecal administration.

Elements of the approach outlined here are scattered in the literature but have not been integrated into an explicit therapeutic intervention for several possible reasons: (a) early studies used CAP, which is less effective for cell deletion; (b) vanilloid agonists are generally thought of as algesic agents; and (c) the proposed mechanism(s) of action were either vaguely defined or inconsistent to form a basis for human clinical trials [36, 64, 72-74, 76, 77, 92]. In contrast, the direct observation of RTX action, in real time, on in vitro DRG neurons or

TRPV1-expressing cells provided a visually appreciable mechanism for therapeutic application [18].

The present experiments address an additional key issue in analgesia research, which is the predictive relationship between evaluation of new drugs in experimental models and their eventual performance in human clinical pain, where they are frequently ineffective or only minimally so. The canine model we introduce provides a transitional bridge between nonclinical rodent data and eventual human trials, and reinforces the idea that a treatment will be safe and effective. The canine study also highlights the need for better measurement tools for large-animal studies. The results with RTX were robust enough to be easily rated by the human observers; however, new methods to obtain objective, meaningful measurements should be developed. The selectivity of RTX in live-cell imaging of human DRG neurons provides a second type of translational observation between basic in vitro observations and human clinical application.

These data represent a progressive series of steps from molecular biological, electrophysiological and imaging assisted characterization of TRPV1 to experimental rodent models and clinical veterinary models, to conclude with human cells that explore the clinical potential of selective nociceptive neuronal deletion for pain control. The cell deletion approach may provide an important alternative to present treatments, and its eventual use will help to improve the quality of life in patients with unrelenting pain.

6. NEW FINDINGS

1. Confocal imaging on the TRPV1-eGFP transfected cells depicts the intracellular localization of the vanilloid receptor. It is localized to the plasma membrane ($TPRV1_{PM}$) and to the endoplasmic reticulum ($TRPV1_{ER}$).
2. High-resolution confocal imaging using cells ectopically expressing the TRPV1-eGFP hybrid molecule also report on the immediate cellular events after administration of vanilloid agonists. These comprise ER and mitochondrial fragmentation. The cellular events are terminating in death of the cell by Ca^{2+}-cytotoxic mechanism.
3. The ER localized TRPV1 ($TRPV1_{ER}$) is functionally effective as evidenced by experiments in “zero” extracellular calcium conditions and overlaps with the thapsigargin sensitive intracellular calcium store.
4. Activation of DRG neurons in “zero” extracellular conditions reveals signaling along neuronal axonal and dendritic projections.
5. Peripheral (subcutaneous, perineural) application of RTX leads to *reversible* analgesia by destruction of peripheral nerve endings. The effect is reversible due the regenerative

ability of peripheral nerve fibers and due to the fact that peripheral application of RTX did not reduce the number of TRPV1 positive neurons in the corresponding dorsal root ganglia.

6. Central (close to the neuronal body) application of RTX leads to *irreversible* deletion of TRPV1 expressing pain sensitive neurons.
7. Severe pain including chemical, inflammatory and cancer related pain can be effectively managed by peripheral or central (single intraganglionic or multiganglionic) application of RTX.
8. In vitro data on human dorsal root ganglion cultures suggest that the treatment will be safe and effective in case of human administration.

7. REFERENCES

1. Bernabei, R., et al., *Management of pain in elderly patients with cancer. SAGE Study Group. Systematic Assessment of Geriatric Drug Use via Epidemiology.* Jama, 1998. **279**(23): p. 1877-82.
2. Cleeland, C.S., et al., *Pain and its treatment in outpatients with metastatic cancer.* N Engl J Med, 1994. **330**(9): p. 592-6.
3. Wolfe, J., et al., *Symptoms and suffering at the end of life in children with cancer.* N Engl J Med, 2000. **342**(5): p. 326-33.
4. Eddy, N.B. and E.L. May, *The search for a better analgesic.* Science, 1973. **181**(98): p. 407-14.
5. Nitu, A.N., et al., *Emerging trends in the pharmacotherapy of chronic pain.* Expert Opin Investig Drugs, 2003. **12**(4): p. 545-59.
6. Scholz, J. and C.J. Woolf, *Can we conquer pain?* Nat Neurosci, 2002. **5 Suppl**: p. 1062-7.
7. Cowan, J.D. and D. Walsh, *Terminal sedation in palliative medicine--definition and review of the literature.* Support Care Cancer, 2001. **9**(6): p. 403-7.
8. Cowan, J.D. and T.W. Palmer, *Practical guide to palliative sedation.* Curr Oncol Rep, 2002. **4**(3): p. 242-9.
9. Harrison, P., *Update on pain management for advanced genitourinary cancer.* J Urol, 2001. **165**(6 Pt 1): p. 1849-57; discussion 157-8.
10. Foley, K.M. and H. Gelband, *Improving palliative care for cancer.* Institute of Medicine and National Research Council, 2001(National Academy Press, Washinton, D.C.).
11. Adler, P., *The use of bupivacaine for blocking the Gasserian ganglion in major trigeminal neuralgia.* Int J Oral Surg, 1975. **4**(6): p. 251-7.
12. Goto, F., et al., *The long lasting effects of peripheral nerve blocks for trigeminal neuralgia using high concentration of tetracaine dissolved in bupivacaine.* Pain, 1999. **79**(1): p. 101-3.
13. Pollock, B.E., et al., *High-dose trigeminal neuralgia radiosurgery associated with increased risk of trigeminal nerve dysfunction.* Neurosurgery, 2001. **49**(1): p. 58-62; discussion 62-4.
14. Richardson, J.D. and M.R. Vasko, *Cellular mechanisms of neurogenic inflammation.* J Pharmacol Exp Ther, 2002. **302**(3): p. 839-45.
15. Tominaga, M., et al., *The cloned capsaicin receptor integrates multiple pain-producing stimuli.* Neuron, 1998. **21**(3): p. 531-43.
16. Caterina, M.J., et al., *The capsaicin receptor: a heat-activated ion channel in the pain pathway.* Nature, 1997. **389**(6653): p. 816-24.
17. Szallasi, A. and P.M. Blumberg, *Resiniferatoxin, a phorbol-related diterpene, acts as an ultrapotent analog of capsaicin, the irritant constituent in red pepper.* Neuroscience, 1989. **30**(2): p. 515-20.
18. Olah, Z., et al., *Ligand-induced Dynamic Membrane Changes and Cell Deletion Conferred by Vanilloid Receptor 1.* J Biol Chem, 2001. **276**(14): p. 11021-11030.
19. Macrae, W.A., *Chronic pain after surgery.* Br J Anaesth, 2001. **87**(1): p. 88-98.
20. Olah, Z., et al., *A cloning and epsilon-epitope-tagging insert for the expression of polymerase chain reaction-generated cDNA fragments in Escherichia coli and mammalian cells.* Anal Biochem, 1994. **221**(1): p. 94-102.
21. Acs, G., et al., *Distinct structure-activity relations for stimulation of 45Ca uptake and for high affinity binding in cultured rat dorsal root ganglion neurons and dorsal root ganglion membranes.* Brain Res Mol Brain Res, 1996. **35**(1-2): p. 173-82.

22. Szabo, T., et al., *Epidural resiniferatoxin induced prolonged regional analgesia to pain.* Brain Res, 1999. **840**(1-2): p. 92-8.
23. Endrenyi, L., C. Fajszi, and F.H. Kwong, *Evaluation of Hill slopes and Hill coefficients when the saturation binding or velocity is not known.* Eur J Biochem, 1975. **51**(2): p. 317-28.
24. Hough, C.J., et al., *Carbamazepine inhibition of N-methyl-D-aspartate-evoked calcium influx in rat cerebellar granule cells.* J Pharmacol Exp Ther, 1996. **276**(1): p. 143-9.
25. Grynkiewicz, G., M. Poenie, and R.Y. Tsien, *A new generation of Ca2+ indicators with greatly improved fluorescence properties.* J Biol Chem, 1985. **260**(6): p. 3440-50.
26. Hargreaves, K., et al., *A new and sensitive method for measuring thermal nociception in cutaneous hyperalgesia.* Pain, 1988. **32**(1): p. 77-88.
27. Iadarola, M.J., et al., *Differential activation of spinal cord dynorphin and enkephalin neurons during hyperalgesia: evidence using cDNA hybridization.* Brain Res, 1988. **455**(2): p. 205-12.
28. Benoliel, R., et al., *Actions of intrathecal diphtheria toxin-substance P fusion protein on models of persistent pain.* Pain, 1999. **79**(2-3): p. 243-53.
29. Kedei, N., et al., *Analysis of the native quaternary structure of vanilloid receptor 1.* J Biol Chem, 2001. **276**(30): p. 28613-9.
30. Subramanian, K. and T. Meyer, *Calcium-induced restructuring of nuclear envelope and endoplasmic reticulum calcium stores.* Cell, 1997. **89**(6): p. 963-71.
31. Karai, L.J., et al., *Vanilloid receptor 1 regulates multiple calcium compartments and contributes to Ca2+-induced Ca2+ release in sensory neurons.* J Biol Chem, 2004. **279**(16): p. 16377-87.
32. Jancso, N., A. Jancso-Gabor, and J. Szolcsanyi, *Direct evidence for neurogenic inflammation and its prevention by denervation and by pretreatment with capsaicin.* Br J Pharmacol, 1967. **31**(1): p. 138-51.
33. Holzer, P., *Neurogenic vasodilatation and plasma leakage in the skin.* Gen Pharmacol, 1998. **30**(1): p. 5-11.
34. Bhave, G., et al., *cAMP-dependent protein kinase regulates desensitization of the capsaicin receptor (VR1) by direct phosphorylation.* Neuron, 2002. **35**(4): p. 721-31.
35. Liu, L. and S.A. Simon, *The influence of removing extracellular Ca2+ in the desensitization responses to capsaicin, zingerone and olvanil in rat trigeminal ganglion neurons.* Brain Res, 1998. **809**(2): p. 246-52.
36. Holzer, P., *Capsaicin: cellular targets, mechanisms of action, and selectivity for thin sensory neurons.* Pharmacol Rev, 1991. **43**(2): p. 143-201.
37. Price, T.J., et al., *The neuronal distribution of cannabinoid receptor type 1 in the trigeminal ganglion of the rat.* Neuroscience, 2003. **120**(1): p. 155-62.
38. Caterina, M.J., et al., *Impaired nociception and pain sensation in mice lacking the capsaicin receptor [see comments].* Science, 2000. **288**(5464): p. 306-13.
39. Davis, J.B., et al., *Vanilloid receptor-1 is essential for inflammatory thermal hyperalgesia.* Nature, 2000. **405**(6783): p. 183-7.
40. Zimmermann, M., *Pathobiology of neuropathic pain.* Eur J Pharmacol, 2001. **429**(1-3): p. 23-37.
41. Kauppila, T., *Correlation between autotomy-behavior and current theories of neuropathic pain.* Neurosci Biobehav Rev, 1998. **23**(1): p. 111-29.
42. Graham DI, L.P., *Greenfield's Neuropathology, Sixth Edition*. Vol. II. 1997. 395.
43. Smart, D., et al., *Characterisation using FLIPR of human vanilloid VR1 receptor pharmacology.* Eur J Pharmacol, 2001. **417**(1-2): p. 51-8.
44. Raymon, H.K., et al., *Immortalized human dorsal root ganglion cells differentiate into neurons with nociceptive properties.* J Neurosci, 1999. **19**(13): p. 5420-8.
45. Szallasi, A., et al., *Vanilloid (capsaicin) receptors in the rat: distribution in the brain, regional differences in the spinal cord, axonal transport to the periphery, and depletion by systemic vanilloid treatment.* Brain Res, 1995. **703**(1-2): p. 175-83.
46. Farkas-Szallasi, T., et al., *Vanilloid receptor loss is independent of the messenger plasticity that follows systemic resiniferatoxin administration.* Brain Res, 1996. **719**(1-2): p. 213-8.
47. Szallasi, A., et al., *The cloned rat vanilloid receptor VR1 mediates both R-type binding and C-type calcium response in dorsal root ganglion neurons.* Mol Pharmacol, 1999. **56**(3): p. 581-7.
48. Acs, G., et al., *Differential activation and desensitization of sensory neurons by resiniferatoxin.* J Neurosci, 1997. **17**(14): p. 5622-8.
49. Biro, T., et al., *Specific vanilloid responses in C6 rat glioma cells.* Brain Res Mol Brain Res, 1998. **56**(1-2): p. 89-98.
50. Biro, T., et al., *Characterization of functional vanilloid receptors expressed by mast cells.* Blood, 1998. **91**(4): p. 1332-40.
51. Szallasi, A., et al., *The stimulation of capsaicin-sensitive neurones in a vanilloid receptor- mediated fashion by pungent terpenoids possessing an unsaturated 1,4- dialdehyde moiety.* Br J Pharmacol, 1996. **119**(2): p. 283-90.
52. Karai, L., et al., *Deletion of vanilloid receptor 1-expressing primary afferent neurons for pain control.* J Clin Invest, 2004. **113**(9): p. 1344-52.

53. Berridge, M.J., P. Lipp, and M.D. Bootman, *The versatility and universality of calcium signalling.* Nat Rev Mol Cell Biol, 2000. **1**(1): p. 11-21.
54. Simpson, P.B. and J.T. Russell, *Role of mitochondrial Ca2+ regulation in neuronal and glial cell signalling.* Brain Res Brain Res Rev, 1998. **26**(1): p. 72-81.
55. Earnshaw, W.C., *Nuclear changes in apoptosis.* Curr Opin Cell Biol, 1995. **7**(3): p. 337-43.
56. Jancso, G. and S.N. Lawson, *Transganglionic degeneration of capsaicin-sensitive C-fiber primary afferent terminals.* Neuroscience, 1990. **39**(2): p. 501-11.
57. Chiba, T., S. Masuko, and H. Kawano, *Correlation of mitochondrial swelling after capsaicin treatment and substance P and somatostatin immunoreactivity in small neurons of dorsal root ganglion in the rat.* Neurosci Lett, 1986. **64**(3): p. 311-6.
58. Sugimoto, T., et al., *Electron microscopic demonstration of nick end-labeled DNA fragments during capsaicin-induced apoptosis of trigeminal primary neurons in neonatal rats [In Process Citation].* Brain Res, 1999. **818**(1): p. 147-52.
59. Choi, D.W., *Calcium-mediated neurotoxicity: relationship to specific channel types and role in ischemic damage.* Trends Neurosci, 1988. **11**(10): p. 465-9.
60. Yu, S.P., et al., *NMDA receptor-mediated K+ efflux and neuronal apoptosis.* Science, 1999. **284**(5412): p. 336-9.
61. McCleane, G., *The analgesic efficacy of topical capsaicin is enhanced by glyceryl trinitrate in painful osteoarthritis: a randomized, double blind, placebo controlled study.* Eur J Pain, 2000. **4**(4): p. 355-60.
62. Caudle, R.M., et al., *Resiniferatoxin-induced loss of plasma membrane in vanilloid receptor expressing cells.* Neurotoxicology, 2003. **24**(6): p. 895-908.
63. Neubert, J.K., et al., *Peripherally induced resiniferatoxin analgesia.* Pain, 2003. **104**(1-2): p. 219-28.
64. Nolano, M., et al., *Topical capsaicin in humans: parallel loss of epidermal nerve fibers and pain sensation.* Pain, 1999. **81**(1-2): p. 135-45.
65. Ossipov, M.H., et al., *Lack of involvement of capsaicin-sensitive primary afferents in nerve-ligation injury induced tactile allodynia in rats.* Pain, 1999. **79**(2-3): p. 127-33.
66. Tender, G.C., et al., *Selective ablation of nociceptive neurons for elimination of hyperalgesia and neurogenic inflammation.* J Neurosurg, 2005. **102**(3): p. 522-5.
67. Kocoglu, H., et al., *Cancer pain, pathophysiology, characteristics and syndromes.* Eur J Gynaecol Oncol, 2002. **23**(6): p. 527-32.
68. Payne, R., *Anatomy, physiology, and neuropharmacology of cancer pain.* Med Clin North Am, 1987. **71**(2): p. 153-67.
69. Wacnik, P.W., et al., *Nociceptive characteristics of tumor necrosis factor-alpha in naive and tumor-bearing mice.* Neuroscience, 2005. **132**(2): p. 479-91.
70. Vollmer-Conna, U., et al., *Production of pro-inflammatory cytokines correlates with the symptoms of acute sickness behaviour in humans.* Psychol Med, 2004. **34**(7): p. 1289-97.
71. Dionne, R.A., et al., *The substance P receptor antagonist CP-99,994 reduces acute postoperative pain.* Clin Pharmacol Ther, 1998. **64**(5): p. 562-8.
72. Jancso, G. and E. Kiraly, *Sensory neurotoxins: chemically induced selective destruction of primary sensory neurons.* Brain Res, 1981. **210**(1-2): p. 83-9.
73. Yaksh, T.L., et al., *Intrathecal capsaicin depletes substance P in the rat spinal cord and produces prolonged thermal analgesia.* Science, 1979. **206**(4417): p. 481-3.
74. Nagy, J.I., P.C. Emson, and L.L. Iversen, *A re-evaluation of the neurochemical and antinociceptive effects of intrathecal capsaicin in the rat.* Brain Res, 1981. **211**(2): p. 497-502.
75. Appendino, G. and A. Szallasi, *Euphorbium: modern research on its active principle, resiniferatoxin, revives an ancient medicine.* Life Sci, 1997. **60**(10): p. 681-96.
76. Iadarola, M.J., et al., *Neural activation during acute capsaicin-evoked pain and allodynia assessed with PET.* Brain, 1998. **121 (Pt 5)**: p. 931-47.
77. Jeftinija, S., et al., *Effect of capsaicin and resiniferatoxin on peptidergic neurons in cultured dorsal root ganglion.* Regul Pept, 1992. **39**(2-3): p. 123-35.
78. Maggi, C.A., et al., *Similarities and differences in the action of resiniferatoxin and capsaicin on central and peripheral endings of primary sensory neurons.* Neuroscience, 1990. **37**(2): p. 531-9.
79. Sweet, W.H., *Deafferentation pain after posterior rhizotomy, trauma to a limb, and herpes zoster.* Neurosurgery, 1984. **15**(6): p. 928-32.
80. Taha, J.M. and J.M. Tew, Jr., *Comparison of surgical treatments for trigeminal neuralgia: reevaluation of radiofrequency rhizotomy.* Neurosurgery, 1996. **38**(5): p. 865-71.
81. Traub, R.J., M.J. Iadarola, and M.A. Ruda, *Effect of multiple dorsal rhizotomies on calcitonin gene-related peptide-like immunoreactivity in the lumbosacral dorsal spinal cord of the cat: a radioimmunoassay analysis.* Peptides, 1989. **10**(5): p. 979-83.
82. Woolf, C.J., P. Shortland, and R.E. Coggeshall, *Peripheral nerve injury triggers central sprouting of myelinated afferents.* Nature, 1992. **355**(6355): p. 75-8.

83. Santha, P. and G. Jancso, *Transganglionic transport of choleragenoid by capsaicin-sensitive C-fibre afferents to the substantia gelatinosa of the spinal dorsal horn after peripheral nerve section.* Neuroscience, 2003. **116**(3): p. 621-7.
84. Bao, L., et al., *Peripheral axotomy induces only very limited sprouting of coarse myelinated afferents into inner lamina II of rat spinal cord.* Eur J Neurosci, 2002. **16**(2): p. 175-85.
85. Pan, H.L., et al., *Resiniferatoxin induces paradoxical changes in thermal and mechanical sensitivities in rats: mechanism of action.* J Neurosci, 2003. **23**(7): p. 2911-9.
86. LaMotte, R.H., L.E. Lundberg, and H.E. Torebjork, *Pain, hyperalgesia and activity in nociceptive C units in humans after intradermal injection of capsaicin.* J Physiol, 1992. **448**: p. 749-64.
87. Ferrell, W.R., F.Y. Lam, and I. Montgomery, *Differences in the axon composition of nerves supplying the rat knee joint following intra-articular injection of capsaicin.* Neurosci Lett, 1992. **141**(2): p. 259-61.
88. Sasamura, T., et al., *Existence of capsaicin-sensitive glutamatergic terminals in rat hypothalamus.* Neuroreport, 1998. **9**(9): p. 2045-8.
89. Marinelli, S., et al., *Capsaicin activation of glutamatergic synaptic transmission in the rat locus coeruleus in vitro.* J Physiol, 2002. **543**(Pt 2): p. 531-40.
90. Szabo, T., et al., *Pharmacological characterization of vanilloid receptor located in the brain.* Brain Res Mol Brain Res, 2002. **98**(1-2): p. 51-7.
91. Mezey, E., et al., *Distribution of mRNA for vanilloid receptor subtype 1 (VR1), and VR1- like immunoreactivity, in the central nervous system of the rat and human.* Proc Natl Acad Sci U S A, 2000. **97**(7): p. 3655-60.
92. Winter, J., et al., *Cellular mechanism of action of resiniferatoxin: a potent sensory neuron excitotoxin.* Brain Res, 1990. **520**(1-2): p. 131-40.

8. ACKNOWLEDGEMENTS

I wish to acknowledge Dr. Zoltan Olah, my tutor and supervisor, who directed my research work at the National Institute of Health for his invaluable help during my Ph.D. studies.

I would like to thank Dr. Michael J. Iadarola, a brilliant thinker and researcher for his mentorship and for providing me with all the facilities needed to carry out my experiments.

I started to work on the effects of capsaicin on C-fiber neurons in the laboratory of Dr. Gabor Jancso as an undergraduate student. I would like to acknowledge him for starting me on the path that may lead to the healing of people suffering from severe pain.